ELSEVIER

Clinical Neurophysiology 118 (2007) 645–668

www.elsevier.com/locate/clinph

Theta EEG dynamics of the error-related negativity

Logan T. Trujillo *, John J.B. Allen *

Department of Psychology, University of Arizona, Tucson, AZ, USA

Accepted 15 November 2006
Available online 16 January 2007

Abstract

Objective: The error-related negativity (ERN) is a response-locked brain potential (ERP) occurring 80–100 ms following response errors. This report contrasts three views of the genesis of the ERN, testing the classic view that time-locked phasic bursts give rise to the ERN against the view that the ERN arises from a pure phase-resetting of ongoing theta (4–7 Hz) EEG activity and the view that the ERN is generated – at least in part – by a phase-resetting and amplitude enhancement of ongoing theta EEG activity.

Methods: Time-domain ERP analyses were augmented with time–frequency investigations of phase-locked and non-phase-locked spectral power, and inter-trial phase coherence (ITPC) computed from individual EEG trials, examining time courses and scalp topographies. Simulations based on the assumptions of the classic, pure phase-resetting, and phase-resetting plus enhancement views, using parameters from each subject's empirical data, were used to contrast the time–frequency findings that could be expected if one or more of these hypotheses adequately modeled the data.

Results: Error responses produced larger amplitude activity than correct responses in time–domain ERPs immediately following responses, as expected. Time–frequency analyses revealed that significant error-related post-response increases in total spectral power (phase- and non-phase-locked), phase-locked power, and ITPC were primarily restricted to the theta range, with this effect located over midfrontocentral sites, with a temporal distribution from ≈150–200 ms prior to the button press and persisting up to 400 ms post-button press. The increase in non-phase-locked power (total power minus phase-locked power) was larger than phase-locked power, indicating that the bulk of the theta event-related dynamics were not phase-locked to response. Results of the simulations revealed a good fit for data simulated according to the phase-locking with amplitude enhancement perspective, and a poor fit for data simulated according to the classic view and the pure phase-resetting view.

Conclusions: Error responses produce not only phase-locked increases in theta EEG activity, but also increases in non-phase-locked theta, both of which share a similar topography.

Significance: The findings are thus consistent with the notion advanced by Luu et al. [Luu P, Tucker DM, Makeig S. Frontal midline theta and the error-related negativity; neurophysiological mechanisms of action regulation. Clin Neurophysiol 2004;115:1821–35] that the ERN emerges, at least in part, from a phase-resetting and phase-locking of ongoing theta-band activity, in the context of a general increase in theta power following errors.

Keywords: Error-related negativity; Event-related potentials; Theta; Oscillations; Phase-resetting; Wavelet

1. Introduction

1.1. The classic vs. synchronization interpretations of the ERN

The error-related negativity (ERN or Ne) is a negative response-locked frontal ERP component occurring ~80–100 ms following commission of response errors (Falkenstein et al., 1991; Gehring et al., 1993), the putative generator of which (Dehaene et al., 1994; Luu and Tucker, 2001; Dikman and Allen, 2000) is the dorsal anterior cingulate cortex (ACC), a region implicated in executive control. The ERN is part of a class of "medial frontal negativities" (Gehring and Willoughby, 2004), which include other negative potentials evoked in response to error feedback stimuli (Miltner et al., 1997; Badgaiyan and Posner, 1998;

* Corresponding authors. Tel.: +1 520 621 7448.
E-mail addresses: logant@u.arizona.edu (L.T. Trujillo), jallen@u.arizona.edu (J.J.B. Allen).

1388-2457/$32.00
doi:10.1016/j.clinph.2006.11.009

Ruschow et al., 2002), response competition (Gehring et al., 1992; Falkenstein et al., 1999), and gambling task losses (Gehring and Willoughby, 2002). These findings have led to the interpretation that the ERN is indicative of error monitoring (Falkenstein et al., 1991, 2000; Gehring et al., 1993) or response competition (Carter et al., 1998) processes.

The classic view of ERPs suggests that phasic bursts of activity in several brain regions are time locked to the stimulus or response, but such bursts are uncorrelated with the background oscillatory EEG activity (cf. Yeung et al., 2004). Challenges to this view propose instead that an ERP is the result of a reorganization and phase-resetting of oscillatory EEG activity following the event of interest (e.g., Basar, 1991; Basar-Eroglu et al., 1992; Makeig et al., 2002). Investigating the ERN specifically, Luu and Tucker (2001) observed the ERN as a theta-band midline oscillation with a source localized to centromedial frontal cortex, including the ACC, a region that exhibits task-related theta-band phase locking in patients with intracranial electrodes (Wang et al., 2005). The induction and maintenance of this theta rhythmic activity may arise from interactions between pyramidal cells and inhibitory interneurons, like those found in the rat hippocampus (Buzsáki et al., 1983; Freund and Buzaki, 1996).

Luu et al. (2004) performed a detailed analysis of error-related theta activity by separately examining the magnitude of phase-locked, non-phase-locked, and total theta (phase- plus non-phase-locked) EEG signal energy (a spectral measure in units of $|\mu V|$) elicited over midfrontal sites during a speeded reaction task. Phase-locked energy indexes oscillations demonstrating relative phase consistency with respect to a reference time point (stimulus or response onset) across trials; non-phase-locked energy indexes oscillations that are relatively inconsistent in phase across trials. Using a bandpass filtering rectification method, Luu et al. (2004) found theta-range increases over midfrontal regions for error and correct trials across all three types of energy (phase-locked, non-phase-locked, and total), but with a preferential increase for error trials. Luu et al.'s data are consistent with the hypothesis that the ERN is an oscillatory process that increases in phase-locking during the commission of errors.

1.2. Difficulties in distinguishing the classic vs. phase-resetting interpretations

In order to experimentally distinguish between the classic and phase-resetting hypotheses, it is necessary to distinguish between two sub-cases of the latter; *pure phase-resetting* and *phase-resetting with enhancement* (Yeung et al., 2004). During *pure phase-resetting*, ongoing oscillatory EEG signals reset phase to enter an increased state of phase-locking in response to stimulus or motor events; however the EEG signal does not increase in amplitude. During *phase-resetting with enhancement*, the phase of ongoing oscillatory EEG resets while simultaneously increasing in amplitude in response to a relevant event. Unfortunately these hypotheses of ERN genesis (classic, pure phase-resetting, phase-resetting with enhancement) cannot be unambiguously distinguished from one another by Luu et al.'s observations. This is because discrete event-related EEG signals that are uncorrelated to background physiological signals can mimic synchronized oscillatory signals in the time–frequency domain (Yeung et al., 2004).

For example, Luu et al.'s findings could be due to the induction of ringing artifact by the bandpass filtering of a phasic ERN response. Luu et al. (2004) show, however, that the theta oscillations are present without ringing artifact in the EEG single-trials (Figs. 2–4 of Luu et al., 2004), and that energy in the theta frequency extends well beyond the ERN window, which cannot be fully accounted for by filtering artifacts (Luu et al., personal communication, 2004). While this observation supports the interpretation of the ERN as an oscillatory process, it does not speak to whether or not an increase in overall EEG amplitude is involved. Luu et al. only examined theta-range signals. It turns out that the phase-reset of an EEG signal can induce total power increases in frequencies near the initial signal base frequency before the reset, while decreasing total power at base frequencies (as demonstrated in Section 1.3.2 below). These total power changes can occur in the absence of an amplitude increase (pure phase-resetting). To test this hypothesis, one would have to examine nearby frequency ranges for evidence of frequency shifts in spectral activity, something that Luu et al. did not do.

Thus distinguishing among these three hypotheses of ERN genesis might be better suited for modern time–frequency measures (such as wavelet transformations) that are less susceptible to bandpass filtering artifacts and that can assess multiple frequency ranges simultaneously. This latter characteristic affords a thorough way to investigate if the ERN arises primarily from theta-range signals, or if it additionally reflects signals within nearby frequency ranges (delta, alpha). Furthermore, these modern methods provide measures that directly assess the degree of phase-resetting and phase-locking of a signal across trials (see Section 2.6). Nonetheless, Yeung et al. (2004) have argued that these methods, when applied *qualitatively*, cannot differentiate unambiguously between the classic and phase-resetting views of the ERN.

Many studies have examined the differences in event-related phase synchronization predicted by the three views (classic, phase-resetting, phase-resetting with enhancement). Unfortunately, modern phase synchronization measures are beset by interpretational difficulties. Yeung et al. time–frequency analyzed ERN responses gathered during a standard flanker task and compared these with similar analyses of simulated data that modeled the ERN as a 'phasic' response. They examined whether spectral power (a measure in units of $|\mu V|^2$) was present in the ERN evoked potential to a greater degree than expected on the classical interpretation. As the number of trials entering

into the ERN average increases, the contribution of non-phase-locked activity to the spectral estimates should tend towards zero, assuming that the phases of this activity are randomly distributed across trials. Hence a greater degree of spectral power than expected in the evoked potential could be taken as evidence of a greater degree of phase-locked oscillations contributing to ERN genesis. Nonetheless, Yeung et al. showed that average ERN responses simulated according to the classic view exhibit a similar degree of phase-locked power as the empirical data.

They also showed that a phasic response can produce a qualitative pattern and degree of event-related phase synchronization (a measure of phase consistency across trials, see Section 2.6) similar to what is observed within their empirical ERN data. Other analyses, including examination of the correlation of ERN amplitude with EEG power and the scalp topography of spectral responses, showed similar difficulties in distinguishing between the classic and partial synchronization hypotheses of ERN genesis. Yeung et al. (2004) conclude that such qualitative time–frequency analyses are ambiguous tests of these two hypotheses.

1.3. The present study: overview

The present study implements the suggestion by Yeung et al. (2004) that the ambiguity of time–frequency measures may be removed through *quantitative* analysis of the spread of spectral activation across time and frequency under different hypotheses of ERN generation. Quantifying the time–frequency spread of spectral activity is important because the component processes predicted by each hypothesis may be identified by differentiable time–frequency patterns. The remainder of this section will briefly discuss some possible time–frequency patterns each hypothesis might predict.

1.3.1. The classic hypothesis

Fig. 1A (left) shows a 5 Hz half-cycle cosine wave that had been used before to model single-trial ERN responses produced according to the classic hypothesis (Yeung et al., 2004). Fig. 1A (right) shows the associated wavelet-based total spectral power (see Sections 2.6 and 2.7 for details about all simulations and wavelet transformations). Note that the spectral power has a distinctive triangular shape in time and frequency, with a wide base at lower frequencies and a narrow peak at high frequencies. Also note that there is significant power at frequencies outside of the base signal frequency (5 Hz); these portions of the spectrum are likely due to onset transients.

Although phase-locked power is equivalent to total power for a single-trial response (see Section 2.6), it is clear to see that if amplitude and/or phase-locking are high, the grand-average of many such classic responses should result in a pattern of phase-locked power similar to the basic triangular time–frequency shape of Fig. 1A (modulo any distorting effects due to noise). Measures of phase-locking, such as inter-trial phase coherence (ITPC; see Section 2.6), should also show a similar pattern. Low amplitude and/or phase-locking should produce classic power and ITPC responses of lower amplitude and a greater distortion of the basic triangular shape of the classic time–frequency pattern, as signal energies summate over a wider time–frequency interval.

The above considerations therefore predict that if the ERN arises according to the classic hypothesis, then empirical spectral power (total/phase-locked/non-phase-locked) and ITPC should *increase* in a manner resembling the basic triangular time–frequency shape of Fig. 1A.

1.3.2. Pure phase-resetting

Fig. 1B shows a 5 Hz ERN response (same amplitude and latency as Fig. 1A) simulated according to the pure phase-resetting hypothesis. It has been argued that pure phase-resetting can be empirically distinguished from either the classic or phase-resetting plus enhancement mechanisms by demonstrating event-related phase changes in the EEG without corresponding increases in the spectral power of the ERP (Makeig et al., 2002; Yeung et al., 2004; although see Klimesch et al., 2004). An absence of spectral power changes is not necessarily evidence for pure phase-resetting, however. The reason for this is that a change in phase of a signal necessitates a change in frequency of that signal, and the latter affects the frequency ranges in which event-related power changes will occur.

For example, let $d\phi/dt$ be the change in phase ϕ with respect to time of some sinusoidal signal G defined over time t with amplitude A, base frequency f, and phase ϕ, i.e. $G(t) = A \cdot \sin(2\pi \cdot f \cdot t + \phi)$. To a first approximation, the argument of the sinusoid function describing the phase-changing signal is then $2\pi \cdot f \cdot t + \phi = 2\pi \cdot f \cdot t + (d\phi/dt) \cdot t = 2\pi \cdot F \cdot t$. It follows that the signal frequency during the phase change given by the spectral transformation will be $2\pi \cdot F = 2\pi \cdot f + d\phi/dt$, or $F = f + (1/2\pi) \cdot d\phi/dt$; thus $F < \text{or} > f$, for $d\phi/dt \neq 0$. This result indicates that in the case of phase-resetting without corresponding amplitude changes, the spectral power must *decrease* at the base frequency of the signal and *increase* in nearby frequencies.

Fig. 1B shows an example of a pure phase-reset signal (left column) and the associated total power spectrum. The latter confirms that total power of a phase-reset signal decreases in the base frequency range. The fact that previous studies claiming evidence of pure phase-resetting found event-related phase changes in the EEG without corresponding increases in spectral energy may indicate either that such phase-resetting was weak (i.e. $d\phi/dt \approx 0$), or that signal amplitudes at base frequencies did in fact increase just enough to offset the power decrease due to the phase change (i.e. phase-resetting with enhancement; see below).[1]

[1] As mentioned in Section 1.2, Luu et al. (2004) did not examine total energy within nearby frequency ranges, so it remains possible that the energy increases they observed were due to changes induced by phase-resetting in nearby frequencies in the manner illustrated by Fig. 1C. Yeung et al. (2004) examined phase-locked responses over a wider frequency range, but they did not report total or non-phase-locked power.

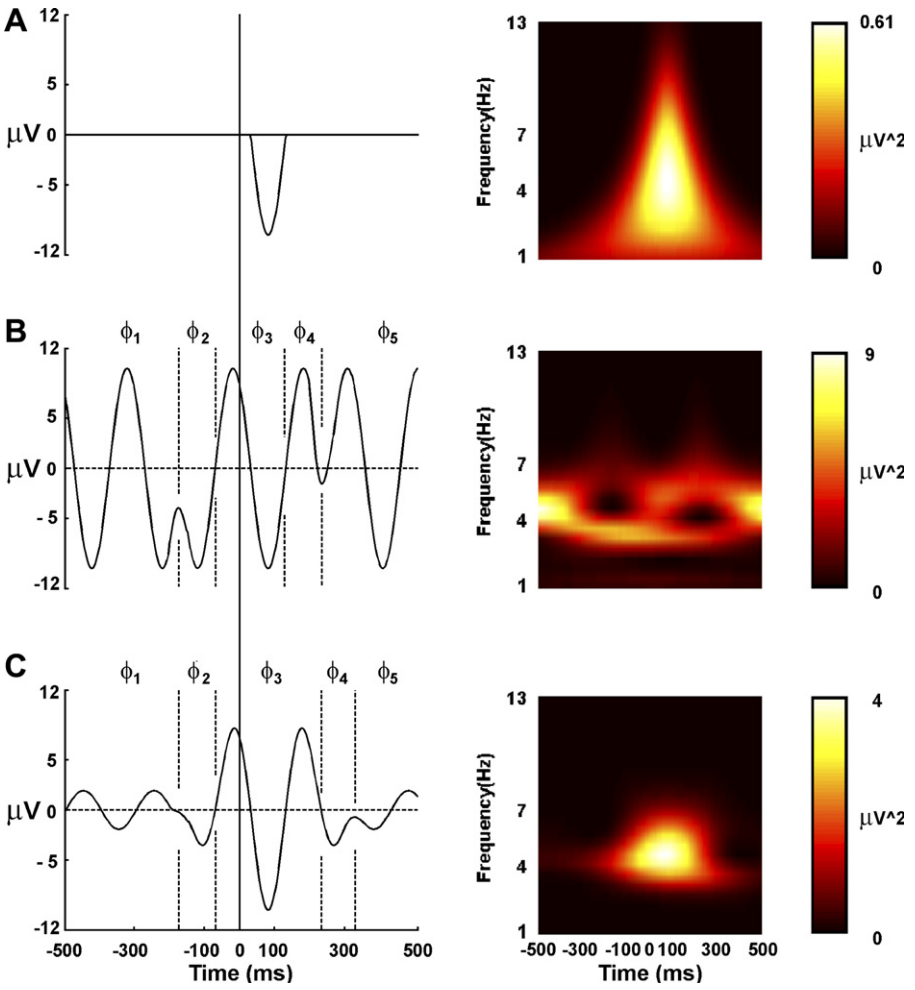

Fig. 1. Left column: Basic oscillatory waveforms used to simulate ERN responses according to the (A) *classic*, (B) *pure phase-resetting*, and (C) *phase-resetting with enhancement* hypotheses of ERN generation. Right column: Corresponding non-baseline-corrected wavelet-based time–frequency representations of these waveforms. The procedures used to create these waveforms and time–frequency representations are described in Sections 2.6 and 2.7.

These above considerations therefore predict that if the ERN arises from pure phase-resetting of ongoing oscillatory EEG signals, then total power should *decrease* in a manner resembling the pattern of decreases in Fig. 1B.

1.3.3. Phase-resetting with enhancement

Fig. 1C shows a 5 Hz ERN response (same amplitude and latency as Fig. 1A and B) simulated according to the phase-resetting plus enhancement hypothesis. This hypothesis suggests that the time–domain ERN signal should be composed of a successive sequence of peaks and troughs characteristic of oscillatory activity with the amplitude increasing and then decreasing with respect to some base level over the duration of the ERN response (Fig. 1C, left). Such activity may onset substantially earlier than the ERP peak latency of the averaged ERN response and may persist for a significant time period afterward, as suggested by the data of Luu et al. (2004). Furthermore, this oscillatory activity must change or reset phase during the transition from the preceding background oscillations to onset of the ERN and then stay relatively phase-locked throughout the ERN peak response before the phase drifts back to background distributions (see dashed lines in Fig. 1C, left).

The pattern of total power contained within such a waveform (Fig. 1C, right) is strikingly different from the patterns associated with either classic or pure phase-resetting signals. Total power activation is restricted to a narrow range around the base frequency of the response, but remains extended in time; the qualitative appearance is almost circular, as opposed to the triangular shape seen for the classic responses (Fig. 1A). In addition the total power magnitude is much greater than for classic power, although less than pure phase-resetting power (note that each signal has equivalent peak amplitude and latency). This difference in power probably arises from the fact that an oscillatory signal possesses a larger temporal extension than a classic signal, and thus more signal energy is present over a given temporal duration. These considerations also suggest that, for an equal level of phase-locking, the non-phase-locked power should be greater for an oscillatory

response than for a phasic response. The presence of phase-resetting, however, will also modify spectral activity by reducing total power responses at the base signal frequency, as seen in Section 1.3.2 above.

Therefore, if the ERN arises from the phase-resetting with enhancement of ongoing oscillatory EEG signals, then empirical spectral power (total/phase-locked/non-phase-locked) and ITPC should *increase* in a manner resembling the basic time–frequency pattern of Fig. 1C.

1.4. The present study: testing hypotheses of ERN generation

This paper tested the predictions discussed in Section 1.3 above using a wavelet-based time–frequency analysis applied to (1) error and correct trials gathered during a typical flanker task that varied in motivational incentive, and (2) ERN responses simulated according to the classic, pure phase-resetting, and phase-resetting with enhancement hypotheses. The three hypotheses of ERN genesis were then assessed by fitting the time–domain and time–frequency properties of the model data to the empirically gathered ERN signals (Sections 2.6 and 2.7). The present analysis was also refined by matching error and correct EEG trials for confounding factors (the total number of trials, reaction time, and degree of ocular activity; see Section 2.4.1) that almost always differ between conditions and thus potentially introduce additional variability into the EEG signals across accuracy conditions. Using these methods, it is quantitatively shown that phase-resetting plus enhancement provides a better model of the empirical data than either the classic view or the pure phase-resetting view; that is, the ERN indeed arises from an amplitude increase and phase-reset of theta-range oscillatory EEG activity. In this manner, the present report extends the approaches of Luu et al. (2004) and Yeung et al. (2004).

2. Methods

The present data were previously reported, as time–domain averaged ERPs, in an analysis of the effects of motivational incentive and participant socialization on the ERN evoked potential response (Dikman and Allen, 2000). Since these factors are not of interest in the present analysis of ERN genesis, the data were collapsed across them for all ERP and time–frequency analyses reported here (see Sections 2.5 and 2.6). Nonetheless, these factors did play roles in participant selection, experimental procedure, behavior, data preprocessing, and matching of trials in terms of confounding variables; thus the significance of motivation and socialization to the performance of these methodological steps will be discussed in the relevant sections (2.1–2.4.1; 3.1) below.

2.1. Participants

From among the 30 participants reported in Dikman and Allen (2000), archival data were available for 21, thus comprising the current sample. Subjects were selected from among 2244 participants who completed the 54-item California Psychological Inventory socialization scale (SO), which was administered during two semesters as part of a requirement for research participation. Low-socialized participants ($n = 9$, mean SO score $= 19.4 \pm 1.6$) scored in the lowest 3% of all scores, whereas high-socialized participants ($n = 12$, mean SO score $= 47.9 \pm 0.5$) scored in the highest 3% of all scores.

2.2. Stimuli and procedure

Following preparation for psychophysiological recording, participants were administered a version of the Eriksen Flankers task (1974), which consisted of identifying the middle character (via a button press) of a 5-letter string of characters that was either compatible or incompatible with the central letter ('SSSSS', 'HHHHH', 'SSHSS', and 'HHSHH'). Characters were displayed unmasked for 52 ms in a standard green font on a black background, and subtended 1.6° of visual angle horizontally and 0.63° vertically. A small fixation symbol (*) was placed ≈ 0.32° below the center character of the letter string and was present on the screen at all times except during feedback.

Participants responded to a central 'S' by pressing the button in one hand and to the 'H' with the other hand, with hand-letter assignment switched during a short rest period every 80 trials. Participants were instructed to correct themselves if they thought they had made a mistake.

Participants completed two conditions, in counterbalanced order, with each in a blocked fashion such that the first 640 trials were one condition, and the second 640 trials the other. In the punishment (PUN) condition, participants received a 95-dB 1-s tone after any trial in which the final response was incorrect, or when no response was made. No tone was delivered following correct trials, including those during which participants had self-corrected. In the reward (REW) condition, participants were informed that for each correct answer they would be credited with a small amount of money, and that they could earn up to $5.00. Participants saw the message ("NO $") on the monitor following incorrect trials, and no feedback following correct trials, including those during which participants had self-corrected. Self-correction to avoid punishment or lack of reward was accomplished by subsequently pressing the correct button within the 1400 ms response window following stimulus onset.

Feedback signals (tone or "NO $") were presented following uncorrected errors 1465 ms after stimulus offset in both conditions, regardless of response latency. Correct responses and self-corrected errors did not result in feedback. Because only self-corrected error trials were included in the analyses, this feedback stimulus did not influence any of the waveforms presented and analyzed in this manuscript.

2.3. Behavioral analysis

Individuals' accuracy and reaction time was computed for all Error and Correct trials for each feedback condition, and then averaged across participants. Potential between-condition differences were statistically assessed via a 2×2 (Error/Correct × Punishment/Reward) mixed-model ANOVA.

2.4. EEG recording and initial data pre-processing

EEG was recorded from 25 scalp sites via an electrode cap. Eye movements and blinks were recorded from electrooculographic (EOG) sites on the face: two sites ≈2 cm below the center of fixation for each eye, and one from an electrode placed on the nasion. All EEG and EOG channels were referenced to A1 on-line, and re-referenced off-line to linked mastoids. All EEG and EOG impedances were less than 5 kΩ. EEG was amplified 20,000 times, and digitized at 256 Hz continuously. EEG was filtered on-line at 0.01 and 100 Hz. EOG signals and EEG sites FP1 and FP2 were amplified 5000 times.

Eye movements and blinks were corrected via a regression procedure (Semlitsch et al., 1986) implemented within the Neuroscan 4.2 software package (Neurosoft Inc., Sterling VA, USA). Muscle artifacts were identified in the raw EEG record by visual inspection, and marked using the Neuroscan software so that trials containing any portion of these artifacts would not be included in further analysis. Artifact-corrected continuous EEG files were segmented into 3200 ms epochs starting 1950 ms prior to, and ending 1250 ms after, the response. In the case of self-corrected errors, epoch timing was defined by the first (and incorrect) response. Epochs were sorted into the four possible combinations of Accuracy (Error/Correct) and Feedback Condition (Punishment/Reward) for each individual and type of filtered data (but subsequently collapsed across feedback condition).

2.4.1. Matching of trials in terms of confounding variables

Because there was a large difference in the number of trials and reaction times between the error and correct trials for both the punishment and reward conditions (see Table 1), it was possible that such large differences in reaction time and trial number could lead to across-condition differences in signal-to-noise ratios of ERP and theta-band amplitudes. This in turn could lead to artifactual differences (or lack thereof) across trial type comparisons. To circumvent this difficulty, each epoch type was matched for reaction time and total number of trials. In addition, each condition was also matched for the presence of eye movements and blinks within the 500 ms post-response period. Although the electrical artifacts resulting from ocular activity were removed from the raw EEG data using a regression procedure described above, it is possible that the neural consequences of such activity could lead to between-condition differences in theta amplitude. This is especially relevant given that the frontal cortex – the locus of the ERN – also contains the frontal eye fields, a region implicated in the initiation of eye movements (Leigh and Zee, 1991). Ocular motion and blinks were identified by examining the EOG of all trials (the EOG channel was left uncorrected for this purpose). Trials containing EOG signals >75 mV or <−75 mV were deemed significantly contaminated with ocular activity, and a count was made for each individual of the total number of trials containing such ocular contamination.

Table 1
Unmatched and matched trial type characteristics

Trial type characteristics	Trials (±SE)	RT (in ms) (±SE)	Ocular activity (% trials) (±SE)
Unmatched values			
Pun Error	59 (6)	421 (13)	39 (8)
Pun Correct	537 (9)	476 (11)	53 (6)
Rew Error	65 (6)	416 (12)	37 (7)
Rew Correct	550 (8)	478 (13)	52 (6)
Matched values			
Pun Error	59 (6)	421 (13)	39 (8)
Pun Correct	57 (5)	424 (12)	39 (7)
Rew Error	65 (6)	417 (12)	44 (8)
Rew Correct	62 (6)	423 (12)	41 (7)

The matching of reaction time, trial number, and eyeblink presence was achieved via an automatic algorithm written specifically for this purpose using Matlab computing software (The MathWorks, Natick, MA, USA). First, reaction times were matched, separately for reward and punishment, so that correct and error trials would be selected with equivalent reaction times within each feedback condition (REW or PUN). For each individual's combination of accuracy and feedback condition, the interval between their maximum and minimum reaction times was divided into 50 ms bins. Trials were assigned to a bin if the bin interval contained a trial's associated reaction time. Next, for a given bin, trials were sorted according to the presence or absence of ocular activity, and Error and Correct trials were paired according to how they matched in terms of this activity. For some individuals and conditions at a given bin, there were more Correct trials containing ocular activity than Error trials. In this case, Correct trials were selected at random using the Matlab random number generator functions until Error and Correct trials were matched according to number of trials containing ocular activity. If there were fewer Correct trials containing ocular activity than Error trials, all of the Correct trials were retained. In either case, the remaining ocular activity-absent Error and Correct trials were then paired at random until either the two trial types matched in total number of trials, or the total number of remaining Correct trials was exhausted for a given bin.

Because it was seldom possible to match Error and Correct trials precisely in terms of reaction time and ocular activity, the success of the matching procedure was assessed by three one-way repeated measures ANOVAs, one for blinks, one for reaction time, and one for number

of trials. No differences were revealed (all $ps > 0.3$; for values see Table 1). These matched epochs were then used for all subsequent electrophysiological analyses reported in this paper.

2.5. ERP analysis

As mentioned earlier, participant socialization and motivation were not germane to the present analysis, and thus the data were collapsed across these conditions for all ERP and time–frequency (Section 2.6) analyses reported in this paper. Note that this procedure still preserves the matching in terms of confounding variables described in Section 2.4.1 above. For the time–domain ERP analyses, the sorted and equated 3200 ms epochs were bandpass filtered between 0.1 and 15 Hz (wide-band) for one set of analyses, and 3–13 Hz (narrow-band) for another, using 385 point finite impulse response (FIR) filters with zero phase distortion, half-amplitude attenuation at the stated frequencies, and transition bands narrower than 1 Hz on either side of the half-amplitude frequency. All epochs were truncated after filtering to the interval −500 to +500 ms with respect to response, eliminating any edge-effects resulting from the temporal extension of the filter window. The filtered epochs were averaged for each individual participant. Wide-band- and narrow-band-filtered epochs were baseline-corrected to the −400 to −300 ms pre-response interval (similar to Luu et al., 2004) to account for the observed temporal extension of the theta oscillations (see Section 3.4) and for ease of comparison with the wavelet-transformed data (see Sections 2.6, 3.3 and 3.4).

Site CZ was chosen for statistical analysis based on the earlier findings of Dikman and Allen (2000) of a central locus for the ERN response. Statistical differences were assessed via non-parametric permutation *T*-tests, corrected for multiple comparisons across successive time points (for a full description of these tests, see Section 2.6 below). Statistical tests of the wideband responses were carried out over the −100 to +100 ms post-response interval (the central portion of the ERN peak) on a time point by time point basis. Since the narrow-band filtered ERN was found to extend over a wide pre-/post-motor response time interval (see Section 3.4), theta-band responses were tested over the −300 to +400 ms period. The statistical results were graphically displayed alongside the grand-average ERPs created by averaging individual ERPs at CZ across participants (within each condition and filter type). ERN scalp topography was visualized by first extracting the difference amplitudes for all electrodes at the ERN latency for each condition. These scalp amplitude distributions were displayed using an algorithm adapted from the EEGLAB toolbox (Delorme and Makeig, 2004) for the Matlab computing software.

2.6. EEG time–frequency analysis

Spectral responses were computed via a wavelet-based time–frequency analysis using in-house scripts written for the Matlab computing software. Raw EEG data were convolved with complex Morlet wavelets (Mallat, 1999; Addison, 2002) to yield the wavelet transform $W(t,f)$. The wavelets were of the form

$$\Phi(t,f) = \frac{1}{\sqrt{\pi^{1/2}\sigma_t}} \exp\left(\frac{-t^2}{2\sigma_t^2}\right)\left\{\exp(i2\pi ft) - \exp\left(\frac{-\alpha^2}{2}\right)\right\} \quad (1)$$

where σ_t is the standard deviation in the time domain around the central frequency f, and the parameter α characterizes the fundamental time/frequency scale of the wavelet. The form of the wavelets used in this study includes a correction factor needed to ensure that they have finite energy (Addison, 2002). The wavelets were normalized such that their total energy was equal to unity. These wavelets provide a good compromise in the necessary trade-off between time and frequency resolution (Mallat, 1999; Addison, 2002), with precise frequency resolution at lower frequencies and better temporal resolution at higher frequencies. The wavelet standard deviations in the time and frequency domains are related by the uncertainty relationships $\sigma_f = 1/(2\pi\sigma_t)$ (Mallat, 1999) and $\alpha = (f/\sigma_f)$ (Tallon-Baudry et al., 1997).

The value of $\alpha = 4.7$, in the range of the typical choices found in the literature (Addison, 2002), was used to provide wavelets with good temporal resolution. This choice yielded a wavelet duration of $(2\sigma_t) = 1450$ ms at frequency $f = 1$ Hz with a frequency spread of $(2\sigma_f) = 0.43$ Hz, while at frequency $f = 13$ Hz this choice yields a duration of $(2\sigma_t) = 115$ ms with a frequency spread of $(2\sigma_f) = 5.53$ Hz. The wavelet transforms were performed over the 3200 ms interval ranging from −1950 ms pre- to 1250 ms post-response. This interval length accommodated over three wavelet cycles at $f = 1$ Hz, with this number increasing to over 41 cycles at $f = 13$ Hz. The transformed signals were then truncated to −500 ms pre- to 500 ms post-response, removing temporal portions of the transform contaminated by edge-effects that arise from the convolution of two discrete signals (EEG/wavelet) of finite temporal lengths (Addison, 2002).

The resulting complex-valued wavelet transform $W(t,f)$ was then used to compute mean spectral power of the EEG signals across the delta (1–3 Hz), theta (4–7 Hz), and alpha (8–13 Hz) frequency ranges over time. For each participant, two types of mean spectral power were computed first for Error and Correct trials: (1) *phase-locked* power estimating the magnitude of EEG oscillatory responses that demonstrate relative phase consistency across trials with respect to the stimulus, and (2) *total* power estimating both phase-consistent and phase-inconsistent portions of the EEG oscillatory signals. Total and phase-locked power were computed as

$$P(t,f)_{total} = \frac{1}{N} \times \left\{\sum_j |W_j(t,f)|\right\}^2 \quad (2)$$

and

$$P(t,f)_{\text{phase-locked}} = \frac{1}{N} \times \left| \sum_j W_j(t,f) \right|^2 = N \times |W_{\text{ERP}}(t,f)|^2 \quad (3)$$

for $j = 1$ to N epochs. That is, total power was defined by wavelet transformation followed by modulus computation of single-trial EEG responses before summation and squaring, while phase-locked power was defined by transformation and squaring of ERP values created after averaging EEG trials. The power measures were normalized by a constant value derived from the requirement that the wavelets have finite energy (Addison, 2002); this constant value equaled 1.44 for the wavelets used in this analysis. Finally, total and phase-locked power was baseline-corrected by subtracting the average response in a given frequency range over the −400 to −300 ms interval. This choice of baseline interval reduced the possibility that baseline spectral activity would be contaminated by post-response activity as a result of the temporal smoothing effects of the wavelet.[2]

The definitions of Eqs. (2) and (3) were motivated by the triangle inequality for complex numbers, $|\sum_j W_j(t,f)|^2 \leqslant \{\sum_j |W_j(t,f)|\}^2$, which the equations satisfy. This inequality indicates that (non-baseline-corrected) total power is always greater than or equal to (non-baseline-corrected) phase-locked power, reflecting the fact that some phase-inconsistent signals destructively summate during the creation of the ERP and do not contribute to the latter's wavelet transform. In contrast, phase-inconsistent signals do not destructively summate during the computation of total power because the transform and modulus operations are performed on a single-trial basis before averaging. Pure *non-phase-locked* (phase-inconsistent) power was assessed by comparing the difference between total and phase-locked power.

In addition to the spectral amplitude, event-related phase synchronization was assessed via computation of inter-trial phase coherence (ITPC). For $j = 1$ to N trials,

$$\begin{aligned} \text{ITPC}(t,f) &= \frac{1}{N} \times \left| \sum_j W_j(t,f) \Big/ |W_j(t,f)| \right| \\ &= \frac{1}{N} \times \left| \sum_j \exp(i\phi_j(t,f)) \right| \end{aligned} \quad (4)$$

where $\phi_j(t,f)$ is the phase of the wavelet at time t and frequency f. In its standard form ITPC indexes the phase consistency of EEG signals across trials at a given latency (Delorme and Makeig, 2004). ITPC values range from 0 (indicating absence of phase-locking) and 1 (indicating perfect phase synchronization). All ITPC values were baseline-corrected over the same interval as the spectral power values, and were computed for each participant. For graphical display, spectral power and ITPC values were averaged across all participants. The scalp topographies of spectral power and ITPC effects were visualized by mapping error-correct differences over the 50–100 ms ERN range for all electrodes and between-condition comparisons. Scalp topographies were displayed via the same Matlab algorithm adapted from EEGLAB as described earlier for the ERP analyses (Section 2.5).

As with the ERPs, site CZ was chosen for statistical analysis due to the previous finding of maximal ERN activity at this site (Dikman and Allen, 2000), and also because of previous studies suggesting a relationship between the ERN and frontal midline theta processes (Luu and Tucker, 2001; Gehring et al., 2000; Luu et al., 2003; Luu et al., 2004). The statistical distributions of many time–frequency measures, however, are known to deviate from normality (Burgess and Gruzelier, 1999). Therefore statistical differences between Error and Correct responses were analyzed via non-parametric bootstrapping and permutation *T*-tests (Burgess and Gruzelier, 1999; Nichols and Holmes, 2001).

For each time–frequency point and Accuracy condition, significant above-baseline increases in spectral and ITPC activity were first indexed via the bootstrapping procedure. Mean responses over the 100 ms interval (−400 to −300 ms) were calculated for each subject, condition, and frequency. Twenty-one samples (reflecting the number of subjects in this study) were randomly selected (with replacement) across subjects, with the sampling performed separately for each frequency and condition. Mean values calculated for each of 5000 sampling events formed the distribution used to estimate the baseline spectral and ITPC activity for each Accuracy condition. For each distribution of 5000 means computed, the $p < 0.05$ two-tailed cutoff value was such that there were only $(0.025 * 5000) = 125$ values greater than this cutoff value. Observed time–frequency responses exceeding this limit were interpreted as being significantly different from the baseline at the $p < .05$ (two-tailed) level.

Time points containing significant above-baseline activity in either Accuracy condition were next assessed by permutation *T*-tests for between-condition differences. At each significantly active time–frequency point, a distribution of *T*-statistics was computed from 5000 random across-subject permutations of within-subject data interchanges between Accuracy conditions under the null hypothesis (Burgess and Gruzelier, 1999; Nichols and Holmes, 2001). These distributions included the *T*-statistics calculated from the actually observed data (the latter being formed, in a statistical sense, from one possible combination of interchanges).

Bonferroni corrections were not made for the multiple Error/Correct comparisons across time and frequency, as successive data points did not meet the requirements of statistical independence (due to the inherent spread of the wavelet). Instead, the maximum test statistic across all examined time–frequency points was retained at each permutation step to create a distribution of 5000 maximal

[2] With the exception of non-phase-locked responses (see Section 3.7), all non-baseline-corrected time–frequency patterns were identical to their baseline-corrected counterparts, save differences in scale.

T-statistics. Statistical inference at each time–frequency point was based on this distribution of maxima. This avoids the multiple comparisons problem that arises from the numerous tests performed over sequential time steps because these multiple tests are collapsed into a single comparison across maxima (Burgess and Gruzelier, 1999; Nichols and Holmes, 2001). Furthermore, restricting the permutation *T*-tests to time–frequency points indicated by the bootstrapping procedure minimized the influence of small, yet highly reliable differences on the maxima distribution when those differences occurred at time points where there was, in fact, no significant above-baseline activity.

The cutoff *T*-statistic for the maxima distribution represented the $p < 0.05$ probability that a given comparison contained *any* time–frequency point with a *T*-statistic $> T_{\text{cutoff}}$. For the distribution of 5000 *T*-statistics computed, the $p < 0.05$ cutoff value was such that there were only $(0.05 * 5000) = 250$ values greater than T_{cutoff}. All time–frequency points with observed *T*-statistics greater than this cutoff value were considered to contain statistically significant Error vs. Correct response differences. *T*-test comparisons were also performed between total and phase-locked power responses in order to index the amount of non-phase-locked activity present in the data.

2.7. ERN simulations

The primary interest of this study was examination of theta-band dynamics plus any activity spread into nearby frequency ranges (upper delta, alpha). Fig. 2 shows examples of the empirical ERN waveforms that the simulation procedures sought to replicate, in particular the narrow-band (3–13 Hz) ERN (Fig. 2B–D). Inspection of the Error trial ERN waveforms always revealed an oscillatory amplitude increase with a central negative peak surrounded by positive peaks. In contrast, Correct trial narrow-band ERN waveforms tended to display a central positive peak surrounded by negative peaks with the oscillation in rough phase with the Error trial ERN.

Error and Correct EEG data epochs were simulated for each individual participant by adding a basic ERN waveform (Fig. 1) onto uncorrelated background noise. For simplicity, only EEG signals at the CZ maximum were simulated. To match the empirical data, the epochs were sampled at 256 Hz and initially ranged from −1950 ms to 1250 ms; the epochs were later truncated to −500 ms to 500 ms after subsequent wavelet transformation. Error and Correct ERPs were created for each participant and then averaged across participants to form grand-average simulated ERPs. The number of simulated epochs for a given participant and condition corresponded to the number of observed epochs for that participant and condition. Three types of simulated EEG epochs were constructed for each participant and condition; one epoch type reflected the classic hypothesis, another the pure phase-resetting hypothesis, and the third the phase-resetting with enhancement hypothesis.

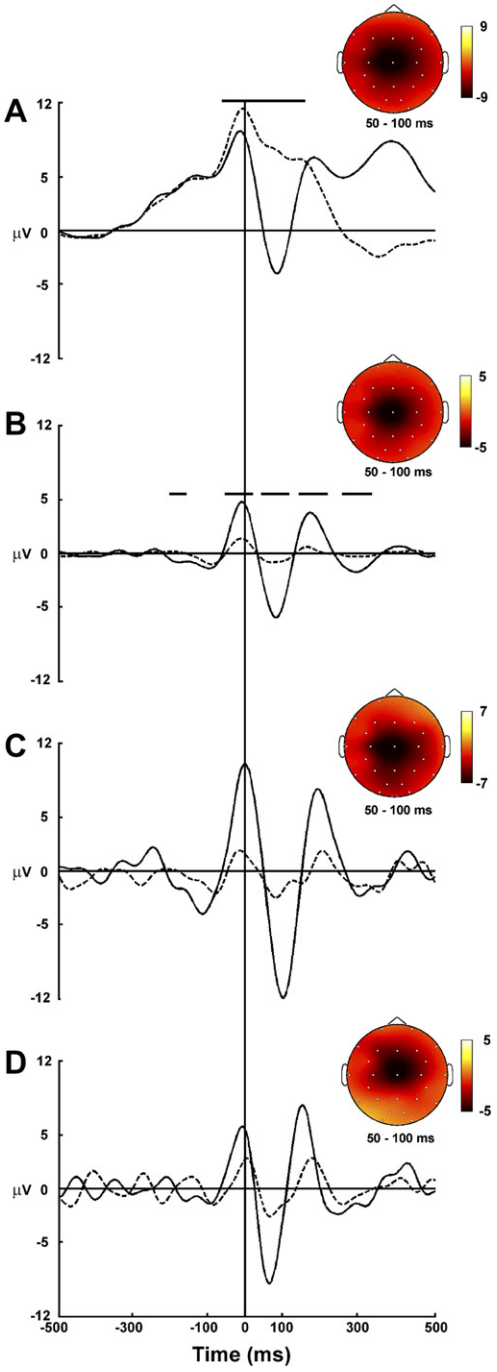

Fig. 2. (A) Grand-average wide-band (0.1–15 Hz) filtered waveforms for *empirical* Error and Correct responses at site CZ. (B) Grand-average narrow-band (3–13 Hz) filtered waveforms for *empirical* Error and Correct responses at site CZ. Solid black line = Error responses, dashed black line = Correct responses, solid horizontal lines = time points containing statistically significant ($p < 0.05$, two-tailed) Error vs. Correct differences. (C and D) Representative ERN evoked potentials from individual participants; solid/dashed lines = Error/Correct. These subjects were selected to illustrate a temporal skew in amplitude increase present in some subjects' data; this feature was explicitly accounted for in the phase-resetting with enhancement model (Section 2.7.3). Insets show Error–Correct ERN difference waveform scalp topography. Light colors indicate positive differences, dark colors indicate negative differences.

2.7.1. Classic simulations

Since classic responses are non-oscillatory, the classic simulations only modeled the central peaks of the Error and Correct trial oscillations to emulate a single phasic peak. For the classic hypothesis (Fig. 1A), the ERN responses were modeled as theta-range half-cycle cosine windows. The base frequencies (f_{base}) of these windows were randomly drawn for each participant and trial from a symmetric distribution centered on the frequency of maximum activity (f_{max}) shared across each participant's total, phase-locked, and ITPC responses. Each distribution of f_{base} ranged continuously over the $f_{max} \pm 2$ Hz interval, with the mean, median, and mode of f_{base} equal to f_{max}. For Error trials, f_{max} was distributed with a mean $= 5.45 \pm 0.18$ Hz, median $= 5.5$ Hz, and mode $= 6$ Hz; for Correct Classic trials, mean $= 4.32$ Hz, median $= 4$ Hz, mode $= 4$ Hz. Error trial peak amplitudes were equal to each participant's largest positive peak-to-negative peak amplitude of the narrow-band (3–13 Hz) Error evoked potentials; Correct trial peak amplitudes were set to be 65% of the Error trial amplitudes.

Latencies were determined from the central peak latency of the individual narrow-band ERNs and were jittered across trials with a spread that varied as

$$\tau = \pm\left(100 - A \cdot \exp\left(\frac{-(f_{base} - f_{max})^2}{2\xi^2}\right)\right) \quad (5)$$

where variables A and ξ parameterize degree of phase-locking and its spread across frequency, respectively. For Error trials, $A = 90$ ms and $\xi = 2$ Hz, with $|\tau| = 10$ ms when $f_{base} = f_{max}$; for Correct trials, $A = 65$ ms, $\xi = 2$ Hz, and with $|\tau| = 30$ ms when $f_{base} = f_{max}$. Note that jittered temporal latency values were converted to sinusoid phase values during the course of the simulation. This variation in latency spread as a function of frequency resulted in maximum phase-locking at the central frequency of each participant and reduced phase-locking at frequencies farther away from the central frequency.

Finally, the basic classic ERN waveform was added to uncorrelated background EEG noise that was simulated by summing together, on each trial, 250 sinusoids spanning the range from 1 to 125 Hz in 0.5 Hz increments. The phases of the sinusoids were randomized between $-\pi$ and π radians separately for each accuracy condition and simulated epoch. For both accuracy conditions, the maximum amplitude of the background EEG was set to be a constant 17.5% of the Error ERN amplitude from 1 Hz up to a cutoff frequency (Error: 10 Hz; Correct: 8 Hz) before decreasing linearly with increasing frequency, with a slope equal to 1/115 of the noise amplitude. This procedure ensured that the noise always had appreciable amplitude in the theta range (~17% of the ERN amplitude on Error trials, and ~26% on Correct trials) before decaying to zero on each trial.

2.7.2. Pure phase-resetting simulations

The pure phase-resetting simulations modeled the full empirical narrow-band oscillatory responses through the temporal concatenation of several partial sinusoid waveforms spanning early, intermediate, central, and late portions of a trial (Fig. 1B). Pure phase-resetting was simulated by using constant amplitude waveforms sharing the same base frequency (f_{base}) but each having a different phase ϕ. In Fig. 1B, the early waveform is labeled with phase ϕ_1, the central waveform is labeled with ϕ_3, and the late waveform is labeled with phase ϕ_5; intermediate waveforms are labeled with phases ϕ_2 and phase ϕ_4. Note that the phase-resetting with enhancement hypothesis in its most general form does not specify in which direction a phase must reset, either through phase advancement or delay. Both possibilities are implemented in the present model by allowing phase values to be both positive and negative. This was motivated by the presence of phase advances and delays in the empirical narrow-band data.

The base frequency (f_{base}) for each sinusoid was randomly drawn for each participant from continuous distributions centered on their individual frequency of maximum activity (f_{max}), as described in Section 2.7.1 above. Error trial f_{base} distributions ranged from $f_{base} = f_{max} \pm 1.5$ Hz; for Correct trials, $f_{base} = f_{max} \pm 1.5$ Hz. In both accuracy conditions, the mean, median, and mode of f_{base} equaled f_{max}. The final frequency of each partial waveform was then determined according to $f_{sim} = f_{base} + (1/2\pi) \cdot d\phi_i/dt$, $i = 1, \ldots, 5$ (see Section 1.3.2). For the central portion of the waveform (Fig. 1B), ϕ_3 was chosen to be constant over time (see further description below), so that $d\phi_3/dt = 0$ and $f_{sim} = f_{base}$. For intermediate waveforms, the values of $d\phi_2/dt$ and $d\phi_4/dt$ were estimated from each participant's narrow-band ERN and the phase values were then defined as $\phi_2 = \phi_3 + (d\phi_2/dt) \cdot t$ and $\phi_4 = \phi_3 + (d\phi_4/dt) \cdot t$, where t is a point in the simulated time interval. The phases of the early and late waveforms were set to be $\phi_1 = \phi_2 \pm \phi_{rand}$ and $\phi_5 = \phi_4 \pm \phi_{rand}$, where ϕ_{rand} was randomly chosen over the continuous interval $(-\pi, \pi)$ separately for ϕ_1 and ϕ_2. Note, however, that since that ϕ_{rand} was a constant over time (although not across trials), $d\phi_1/dt = d\phi_2/dt$ and $d\phi_5/dt = d\phi_4/dt$.

For all participants, the ϕ_3 phases of Error trial central oscillatory sinusoids were chosen so that a negative peak was located at the latency of the central negative peak in the narrow-band Error ERN evoked potential. The ϕ_3 phases of Correct trial sinusoids were chosen so that a positive peak was located at the latency of the central positive peak in the narrow-band Correct ERN evoked potential. These choices were motivated by the appearance of individual participant narrow-band ERN waveforms (Figs. 2B–D). Furthermore, the ϕ_3 phases of the central oscillatory sinusoids were jittered across trials with a spread given by Eq. (5) with $A = 70$ ms, $\xi = (0.5)^{1/2}$ Hz, and $|\tau| = 30$ ms for Error trials when $f_{base} = f_{max}$; for Correct trials, $A = 50$ ms, $\xi = 4$ Hz, and $|\tau| = 50$ ms when $f_{base} = f_{max}$.

The temporal length of the central and intermediate waveforms varied with frequency as $T = (\lambda/2 * f_{sim})$ for $\lambda = 1, 3, 5$, and 7. Odd values of λ were chosen because they

produce oscillations with odd cycle lengths, a prominent feature of our data (see Fig. 2B–D). Integer values of λ were used because they produce oscillations that are zero-valued at their terminal endpoints. The values of λ were generally different for each waveform and participant, being estimated from the latter's narrow-band ERN. To smooth any potential discontinuities at the interface between the early/late and intermediate concatenated waveforms, the waveform values at points within a 100 ms window centered at the interface point were replaced with the waveform values averaged over the original points plus the 10 nearest neighboring points.

The amplitudes of all five waveforms were constant and equal to each participant's largest positive peak-to-negative peak amplitude of the narrow-band (3–13 Hz) Error evoked potentials. Correct trial peak amplitudes were set to be 40% of the Error trial amplitudes. Finally, the concatenated pure phase-resetting waveforms were added to uncorrelated background EEG noise (see Section 2.7.1) on each trial.

The overall pure phase-resetting simulation procedure yielded single-trial oscillatory ERN waveforms that changed in phase several times during an epoch; first during the transition from an early random phase oscillation (ϕ_1) to the first intermediate stage (ϕ_2), to the central oscillation (ϕ_3) phase-locked (with jitter) to a particular latency; and second during the transition from the central latency (ϕ_3) to the second intermediate stage (ϕ_4) and then the late random phase oscillation (ϕ_5). It should be noted that the pure phase-resetting simulation was only approximate in that ϕ_i and/or $d\phi_i/dt$ sometimes changed discontinuously at the points of interface between any two concatenated waveforms; a similar approximation has been used by Klimesch et al. (2004). These discontinuities were probably reduced by the smoothing procedure, the amplitude constraints placed by integer λ values described earlier, and the addition of uncorrelated background noise to the basic ERN waveform. In addition, the smoothing effects of the wavelet transformation likely further minimized the effects of phase discontinuities on the computed time–frequency responses. That such discontinuities were smoothed over is suggested by the smooth nature of the simulated data (e.g., Fig. 1).

2.7.3. Phase-resetting with enhancement simulations

For the phase-resetting with enhancement hypothesis (Fig. 1C), the ERN was again modeled as the temporal concatenation of several partial sinusoid waveforms spanning early, intermediate, central, and late portions of a trial. Phase resetting was simulated by using waveforms sharing the same base frequency (f_{base}) but each having a different phase ϕ_i, $i = 1, \ldots, 5$. In Fig. 1C, the early waveform is labeled with phase ϕ_1, the central waveform is labeled with ϕ_3, and the late waveform is labeled with phase ϕ_5; intermediate waveforms are labeled with phases ϕ_2 and phase ϕ_4.

The base frequency (f_{base}) for each sinusoid was randomly drawn for each participant from distributions centered on their individual frequency of maximum activity (f_{max}), as described in Section 2.7.1 above. Error trial f_{base} distributions ranged from $= f_{max} \pm 1.5$ Hz; for Correct trials, f_{base} ranged from $f_{max} - 0.5$ Hz to $f_{max} + 1.5$ Hz. For the Error condition, the mean, median, and mode of f_{base} equaled f_{max}; for the Correct trials, mean, median, and mode were equal to $1.125 * f_{max}$. The final frequency and phase of each partial waveform was then determined according to $f_{sim,i} = f_{base} + (1/2\pi) \cdot d\phi_i/dt$, as described in Section 2.7.2 above. The lengths of the central and intermediate waveforms then varied as $L = (\lambda/2 * f_{sim})$. The values of λ were the same as used for the pure phase-resetting model described in Section 2.7.2.

For all participants, the ϕ_3 phases of Error trial oscillatory sinusoids were chosen so that a negative peak was located at the latency of the central negative peak in the narrow-band Error ERN evoked potential. The ϕ_3 phases of Correct trial sinusoids were chosen so that a positive peak was located at the latency of the central positive peak in the narrow-band Correct ERN evoked potential (again this choice was motivated by the appearance of the empirical narrow-band waveforms; see Fig. 2B–D). The ϕ_3 phases of the central oscillatory sinusoids were jittered across trials with a spread given by Eq. (5) with $A = 82$ ms, $\xi = (0.5)^{1/2}$ Hz, and $|\tau| = 18$ ms for Error trials when $f_{base} = f_{max}$; for Correct trials, $A = 75$ ms, $\xi = 2^{1/2}$ Hz, and $|\tau| = 25$ ms when $f_{base} = f_{max}$.

Amplitude enhancement of the oscillatory signal was emulated by multiplying the concatenated central and intermediate waveforms by a special window function with a temporal extension equal to the length of the concatenated central and intermediate waveforms. For many participants, the window function consisted of a half-cycle cosine with the peak response centered at the latency of the central negative peak of the ERN. This yielded a symmetric decay in amplitude for data points farther away from the peak in time (Fig. 1C). Some participants, however, had ERN responses in which the central peak and an earlier (Fig. 2C) or later (Fig. 2D) neighboring peak shared similar maximum amplitudes. To simulate data for participants exhibiting this feature, Error and Correct window functions were set to be a constant maximum value over the full duration of the early or late neighboring peak and the corresponding first or second half of the central peak. The window functions over the remaining portions of the central/intermediate sinusoid waveforms were then set to be the first or second portion of a half-cycle cosine window with maximal response at the peak latency of the central waveform. This procedure yielded central waveforms that exhibited full amplitude oscillations throughout the first (or second) half of the waveform until the central peak that decayed in amplitude for the second (or first) half of the waveform.

The maximum amplitudes of Error trials were equal to each participant's largest positive peak-to-negative peak

amplitude of the narrow-band (3–13 Hz) Error evoked potentials. Correct trial peak amplitudes were set to be 50% of the Error trial amplitudes. The amplitudes of the early and late oscillatory waveforms preceding and following the central ERN response were set to the amplitude of the background noise for both trial types.[3] Data were smoothed at the interface between early/late and intermediate concatenated waveforms in the same manner as for the pure phase-resetting simulations (Section 2.7.2). Finally, the concatenated ERN waveforms were added to uncorrelated background EEG noise (see Section 2.7.1) on each trial.

The overall phase-resetting plus enhancement simulation procedure yielded an oscillatory single-trial ERN waveform that changed in phase as it increased from minimum amplitude to a maximum peak and then decreased back to minimum amplitude (Fig. 1C). The oscillatory ERN waveforms changed in phase several times during an epoch; first during the transition from an early random phase oscillation (ϕ_1) to the first intermediate stage (ϕ_2), to the central oscillation (ϕ_3) phase-locked (with jitter) to a particular latency; and second during the transition from the central latency (ϕ_3) to the second intermediate stage (ϕ_4) and then the late random phase oscillation (ϕ_5). Again it should be noted that the effects of any phase discontinuities arising from the approximate phase-resetting model employed here should be smoothed in the overall averages (see Section 2.7.2).

2.7.4. ERN simulation analysis

All simulated data were subjected to the same time–frequency analyses as the empirical data. The resulting time–frequency maps were then compared with time–frequency maps computed from narrow-band filtered empirical data via nonparametric bootstrapping and permutation *t*-tests corrected for multiple comparisons (see Section 2.6). The empirical data were narrow-band filtered for this comparison because (1) the absence of slow wave and high-frequency characteristics in the simulated data would lead to large differences in the lower delta and upper alpha ranges, and these differences could bias the distribution of maxima created for statistical inference, and (2) the bulk of the empirical time–frequency responses were localized within this narrow-band filtered frequency range.

Finally, it is important to state that all of the simulation free parameters were chosen so as to accurately fit the observed ERN characteristics at site CZ. That is, the free parameters were adjusted in a trial-and-error manner so as to produce the most accurate fits (as quantified by the statistical tests) of the simulated evoked potential data to the empirical data. It was not the aim here to simulate the ERN signals from direct consideration of biophysical principles, such as through a dipole model as was done by Yeung et al. (2004). Furthermore, only EEG signals in the theta range and nearby side bands (upper delta and lower alpha) were simulated; lower delta and upper alpha signals present in the observed ERN averages were not simulated (as was also done by Yeung et al., 2004). These signals were neglected in order to simplify the simulation computations and also due to the main focus of this paper on the theta-range. This approach is justified by the fact that this simulation procedure produced results that were reasonably similar to the observed data, modulo the absence of slow wave and high frequency characteristics (see Section 3).

[3] If the constant low-level oscillations prior to and immediately after the main response are taken to reflect the background activity from which the ERN arises, then it is reasonable to assume that their amplitudes are approximately at the level of the noise activity that also contributes to the background oscillations. If that noise has random phases from trial to trial (another reasonable assumption) then the low-level oscillations of the model will be obscured by the noise. It appears that these two assumptions are met in our empirical data, otherwise the oscillations would be noticeable in the baseline of the grand-averages, which they are not (see Fig. 2). The final result of this situation would be a grand-average waveform and time–frequency pattern that looks exactly like those of our original phase-resetting with enhancement model.

3. Results

3.1. Behavioral results

Overall accuracy (before matching of trials for EEG analysis) under Punishment and Reward feedback conditions was 89% ± 1.0% and 88% ± 1.2%, respectively. There were no significant between-condition differences in accuracy ($p > 0.42$). Reaction times (before trial matching) for the Punishment Error and Correct trials were 422 ± 13 ms and 479 ± 13 ms, respectively; Reward Error and Correct reaction times were 417 ± 12 ms and 477 ± 11ms. There was a significant main effect of Accuracy, $F(1,20) = 122.1$, $p < 0.001$, with Error trials significantly faster than Correct trials (Error: 419 ms; Correct: 478 ms). This RT difference was eliminated after trial matching (Table 1).

3.2. ERP analysis

Fig. 2 shows the empirical wide-band (0.1–15 Hz) and narrow-band (3–15 Hz) response-locked ERPs. The wide-band responses (Fig. 2A) showed pronounced ERN peaks within a time interval (50–100 ms), consistent with previously reported time intervals for the ERN. The ERP for the Error condition was significantly more negative than the Correct condition over the entire ERN window, as indicated by the solid horizontal line in Fig. 2A. The scalp topography of the wide-band ERN difference waveform (Fig. 2A, inset) follows what has been reported before (Dikman and Allen, 2000), with a strong focus over midline frontal-central regions and a maximum at CZ.

The narrow-band responses (Fig. 2B) showed pronounced ERN peaks over a large time interval (∼−200 to 300 ms) similar to the theta-band responses observed by Luu et al. (2004). The ERP for the Error condition was significantly greater than the Correct condition over several portions of the ERN response (horizontal lines in Fig. 2B). The frontal-midline scalp topography of the

narrow-band ERN difference waveform (Fig. 2B, inset) also follows what has been reported before (Dikman and Allen, 2000; Luu et al., 2004).

Fig. 2C and D show example narrow-band ERN responses from two participants. Of note is the temporal skew (early/late) in the amplitude increases of these examples. Several subjects did not exhibit this asymmetry; in these cases the peak amplitudes occurred over the central (negative) portion of the response (i.e. Fig. 1C).

3.3. EEG analysis

Fig. 3 shows the baseline-corrected mean spectral power maps computed from unfiltered potentials at site CZ. In the Error trials (top row), total power (left column) and phase-locked power (center column) responses arose around 200 ms pre-motor response and extended until ≈400 ms post-response. Peak activity occurred from 50 to 150 ms in the center of the theta range (5–6 Hz) with some

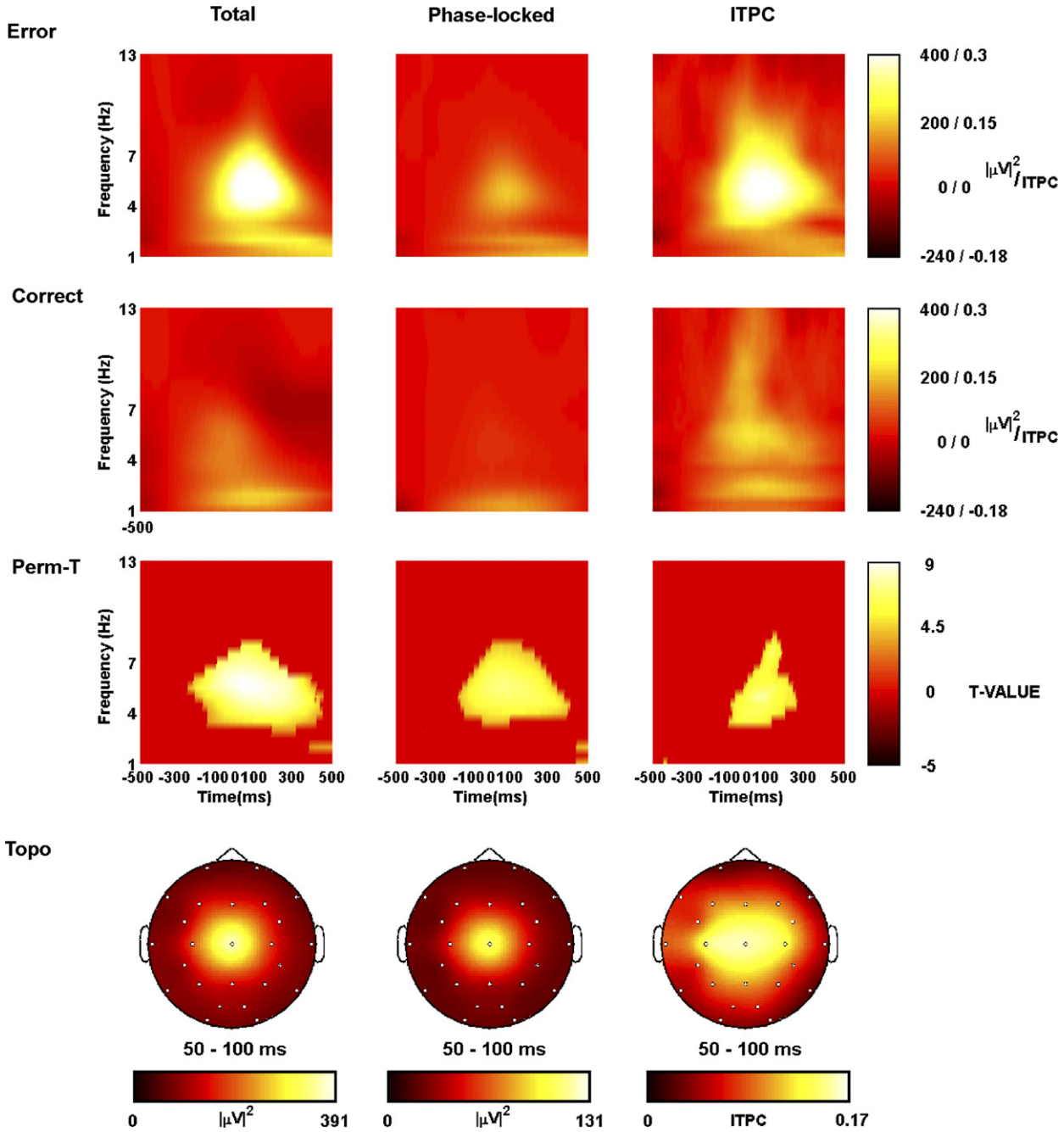

Fig. 3. Baseline-corrected grand-average *empirical* total power (left column), phase-locked power (center column) and ITPC (right column) at site CZ. Light colors indicate increases with respect to the pre-response baseline; dark colors indicate decreases. Top row: Power and ITPC for Error responses. Second row: Power and ITPC for Correct responses. Third row: Error vs. Correct permutation *T*-test statistical comparisons. Light colors indicate positive *T*-values; dark colors indicate negative *T*-values; intermediate colors indicate zero values. All non-zero *T*-values displayed in the figure are significant at the $p < 0.05$ (two-tailed) level. Bottom row: Scalp topography of Error–Correct differences over the indicated interval; Light colors indicate positive differences, dark colors indicate negative differences. Note the differences in scale across total and phase-locked topographic maps.

spreading into the upper delta and lower alpha ranges. Baseline-corrected mean ITPC results (Fig. 3, top row, right column) showed a pattern of responses nearly identical to the spectral amplitudes, with the inter-trial coherence reaching a peak at the same time as the peak spectral amplitude. For Correct responses, by contrast, spectral power responses were greatly reduced in magnitude compared to the Error trials (Fig. 3, second row), and ITPC was similarly reduced.

These between-condition differences were confirmed by the permutation *T*-tests (Fig. 3, third row). The *T*-tests showed that the Error vs. Correct differences lie primarily in the theta range for all three time–frequency measures. In addition to these theta-band differences, there were significant total power differences (Fig. 3, third row, left column) in the upper delta (~3–4 Hz) and lower alpha (~8–10 Hz) ranges from ≈−100 to 400 ms and 0 to 100 ms, respectively. Phase-locked power also demonstrated significant Error vs. Correct differences (Fig. 3, third row, center column) in the extreme upper delta (~3.5–4 Hz) and extreme lower alpha (~8 Hz) ranges. The former activation differences are likely due to Error/Correct differences in the later slow wave characteristics. ITPC responses also demonstrated small "spillover" of significant activation (Fig. 3, third row, right column) from the theta range into the nearby frequency ranges. Also apparent in the figure is that total power responses appear significantly larger than phase-locked power, an effect that was confirmed statistically (see Section 3.7, below).

Finally, the scalp topographies of total, phase-locked, and ITPC theta-range activities (Fig. 3, bottom row; left, center, and right columns, respectively) are similar to that found for the ERN, exhibiting a strong frontal-central focus with a CZ maximum.

3.4. Classic simulations

The classic ERN simulated evoked potentials (Fig. 4, top left panel) appear similar to the empirical ERPs (top right panel), at least over the duration of the central negative peak. Nonetheless, the two waveform types appear to differ in amplitude over the remainder of the time interval. Error and Correct amplitudes significantly differed over the major waveform peaks for the simulated data (solid horizontal lines, Fig. 4, top left panel).

Classic simulation total and phase-locked power (Fig. 4, bottom panel, top and middle rows, first and second columns) displayed triangular time–frequency activation patterns that were similar to the pattern seen for the basic classic waveform of Fig. 1A, yet were greatly reduced in amplitude with respect to the empirical responses.[4] Classic ITPC responses (Fig. 4, bottom panel, top and middle rows, third column) also took on a triangular pattern, and appeared qualitatively to be larger than empirical ITPC responses. Importantly, the classic ERP spectral responses show minimal significant Error/Correct differences (Fig. 4, bottom panel, bottom row) for total power, but phase-locked power and ITPC showed strong differences, again in a characteristic triangular pattern.

The qualitative differences between the classic and narrow-band empirical ERN responses were quantitatively confirmed by the permutation *T*-test comparisons (Fig. 5). The simulated and empirical Error ERN responses were equivalent in magnitude during the central portions of the responses (Fig. 5, left top panel). The two responses significantly differed over the remaining peaks of the oscillation ($p < 0.05$). In contrast, the classic simulation produced a Correct ERN response near identical to that of the empirical data.

The time–frequency measures showed similar discrepancies. Empirical Error condition total theta power (Fig. 5, bottom panel, top row) was greater than classic total theta power over most of the ERN response (~−300 to 300 ms). Empirical Error phase-locked theta power was greater than classic Error phase-locked theta power over small intervals that appear to correspond to the portions of the grand-average ERN oscillation showing the differences between the empirical and classic ERNs (Fig. 5, top left panel). Classic Error phase-locked power, however, was greater than empirical Error phase-locked power in the upper alpha range during the central portion of the ERN evoked potential. This difference was mirrored in the ITPC responses (Fig. 5, bottom panel, top row, right column), which was also greater for classic than empirical data in the upper delta (3–4 Hz) range. Correct empirical and classic total power and ITPC also showed significant differences in the upper delta/lower theta and alpha ranges, respectively. Correct empirical and classic phase-locked power exhibited only small idiosyncratic differences, in agreement with the good fit between the simulated and empirical Correct ERNs.

It should be noted that central peak amplitude differences between the empirical data and classic simulations cannot explain the total and phase-locked theta power differences found during the central response, as the two evoked potentials were not statistically different over the central peak (Fig. 5, top panel). The total power differences are more likely related to the poor fit between the classically simulated and empirical ERNs over the positive peaks neighboring the central negative peak. If the empirical data represent a temporally extended oscillatory process, and thus contain significant ERN activity in time ranges for which there is little-to-no classic activity, then the convolution between the wavelet and the signal will be greatest when the wavelet is centered over all three oscillatory peaks. If the neighboring peaks are absent or reduced in amplitude, as they are for the classic simulation, then the convolution between the wavelet and the classic signal will be reduced relative to the empirical data when the wavelet is positioned over the central response. In contrast, the

[4] Note that this reduced amplitude slightly obscures the triangular pattern of total and phase-locked power displayed in Fig. 4, as the latter is scaled to be consistent with the other figures showing larger magnitude responses, for ease of comparison.

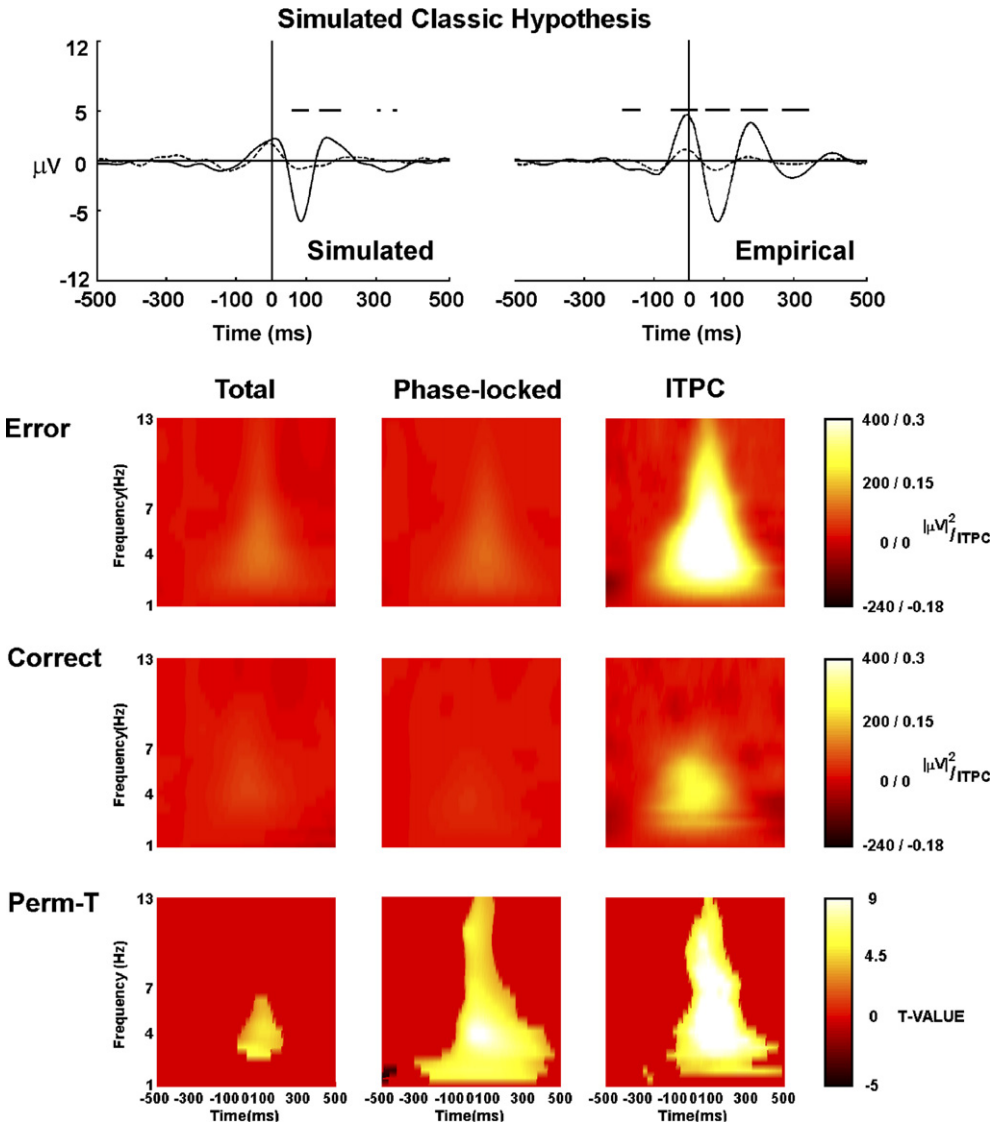

Fig. 4. Results of simulated classic hypothesis. Top panels: Grand-average narrow-band ERN waveforms for Error and Correct responses simulated according to the *classic hypothesis* (left). Grand-average narrow-band empirical ERN waveforms (right). Solid black line = Error responses, dashed black line = Correct responses, solid horizontal lines = time points containing statistically significant ($p < 0.05$, two-tailed) Error vs. Correct differences. Bottom panel: Baseline-corrected grand-average total power (left column), phase-locked power (center column) and ITPC (right column) responses for simulated Error (top row) and Correct data (middle row). Light colors indicate increases with respect to the pre-response baseline; dark colors indicate decreases. Bottom row: Error vs. Correct permutation *T*-test statistical comparisons for simulated data. Light colors indicate positive *T*-values; dark colors indicate negative *T*-values; intermediate colors indicate zero values. All non-zero *T*-values displayed in the figure are significant at the $p < 0.05$ (two-tailed) level.

large amount of high-frequency phase-locked power and ITPC responses present in the classic data is likely due to the characteristic high-frequency offset transients present in the basic classic time–frequency pattern (Fig. 1A).

Since the ERN amplitudes were fixed by the empirical data, the only other way to increase the simulation amplitudes was to increase the overall phase-locking. In additional classic simulations (not shown), increasing the phase-locking of the classical simulations did not improve the overall fit with the empirical data. The central ERN response increased with increased phase-locking to the point that it was significantly greater ($p < 0.05$) than the empirical central ERN peak; the fit between neighboring peaks did not improve appreciably. The high-frequency phase-locked power and ITPC differences increased and spread into lower frequencies. Only the fit between empirical and classic total power was improved by this manipulation.

3.5. Pure phase-resetting simulations

Fig. 6 (top panels) shows narrow-band (3–15 Hz) filtered ERPs simulated according to the phase-resetting hypothesis (top left panel) and for the narrow-band empirical waveforms (top right panel). The morphology of the simulated waveforms is near identical to that of the empirical waveforms, both in terms of peak amplitudes and temporal spread. Significant Error vs. Correct amplitude differences occurred at the same major waveform peaks

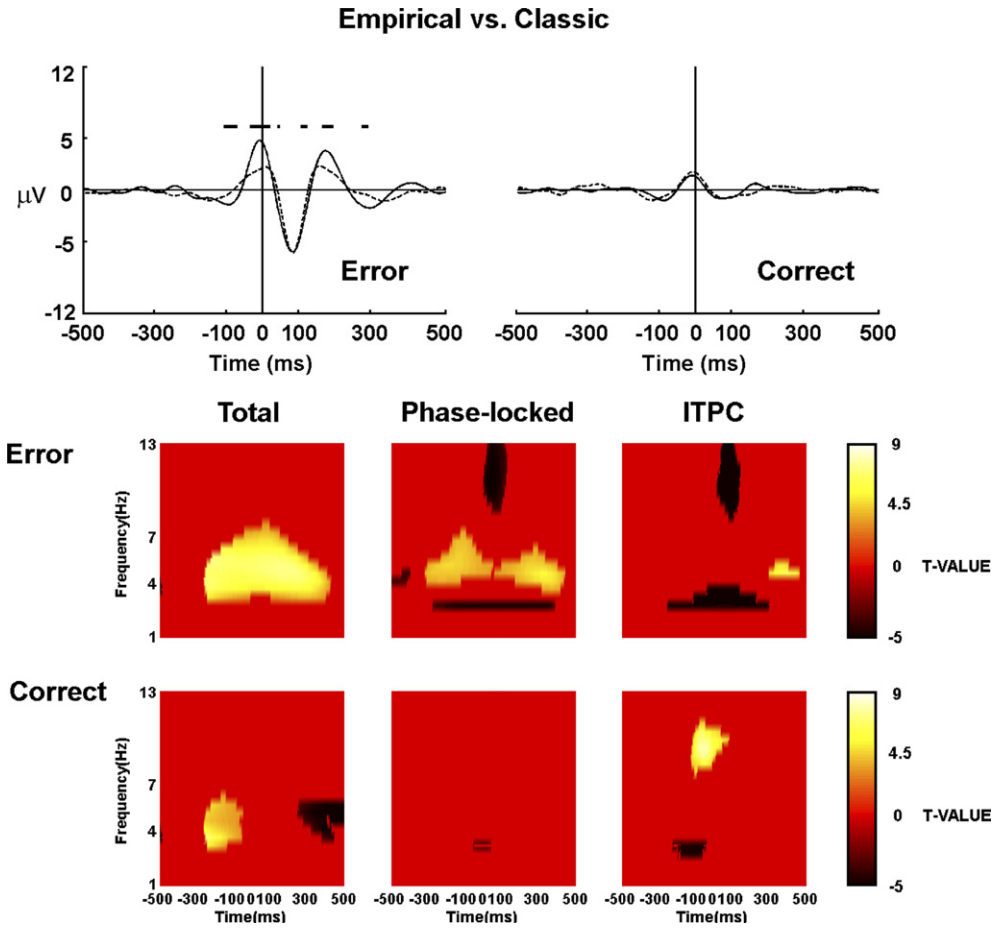

Fig. 5. Quantitative comparison of empirical data and simulated classic hypothesis. Top panel displays time–domain average waveforms: Solid black line = empirical data, dashed black line = simulated data, solid horizontal lines = time points containing statistically significant ($p < 0.05$, two-tailed) Empirical vs. Simulated differences. Lower panel displays permutation T-test statistical comparisons between empirical and *classic* time–frequency responses. Top row: Classic vs. empirical Error responses. Bottom row: Classic vs. empirical Correct responses. Light colors indicate positive T-values; dark colors indicate negative T-values; intermediate colors indicate zero values. All non-zero T-values displayed in the figure are significant at the $p < 0.05$ (two-tailed) level.

in the simulated as the empirical data (solid horizontal lines, Fig. 6, top panels).

Fig. 6 (bottom panel) shows the baseline-corrected time–frequency analyses of the simulated pure phase-resetting trials. Error total power (Fig. 6, bottom panel, top row) shows a theta-range decrease similar to the pattern of Fig. 1B, while Error phase-locked theta power and ITPC both increase with respect to baseline. Correct (Fig. 6, bottom panel, middle row) spectral responses have magnitudes and morphologies that are qualitatively similar to the Correct spectral responses of the empirical waveforms. The spectral responses exhibit patterns of significant Error/Correct differences (Fig. 6, bottom panel, bottom row) that are far different from the empirical differences shown in Fig. 3. Total theta power Error responses do not differ much from the Correct responses. Phase-locked theta power Error/Correct differences are similar to the corresponding empirical differences; however, ITPC Error/Correct differences occur predominantly over a higher frequency range (3–8 Hz) and over a wider temporal extent (~−100 to 300 ms) than the empirical data.

The qualitative similarities between the simulated pure phase-resetting and the empirical ERN evoked potentials were quantitatively confirmed by the permutation T-test comparisons (Fig. 7). Fig. 7 (top panels) compares the narrow-band filtered ERPs simulated according to the phase resetting plus enhancement hypothesis to the narrow-band empirical waveforms for the Error (top left panel) and Correct (top right panel) conditions. The two types of waveforms were nearly identical, only differing over a very small interval at an early stage of the Error response. With respect to the time–frequency responses, however, empirical total Error power was significantly greater than simulated total Error power over the theta range. This difference reflects not only the increase of empirical theta power, but the decrease of pure phase-resetting total power as well. Empirical vs. pure phase-resetting Error phase-locked and ITPC responses were small and restricted to the delta range. Simulated Correct total power was greater than Empirical total power over the 3–7 Hz range from ~−250 to 0 ms. Empirical vs. simulated Correct

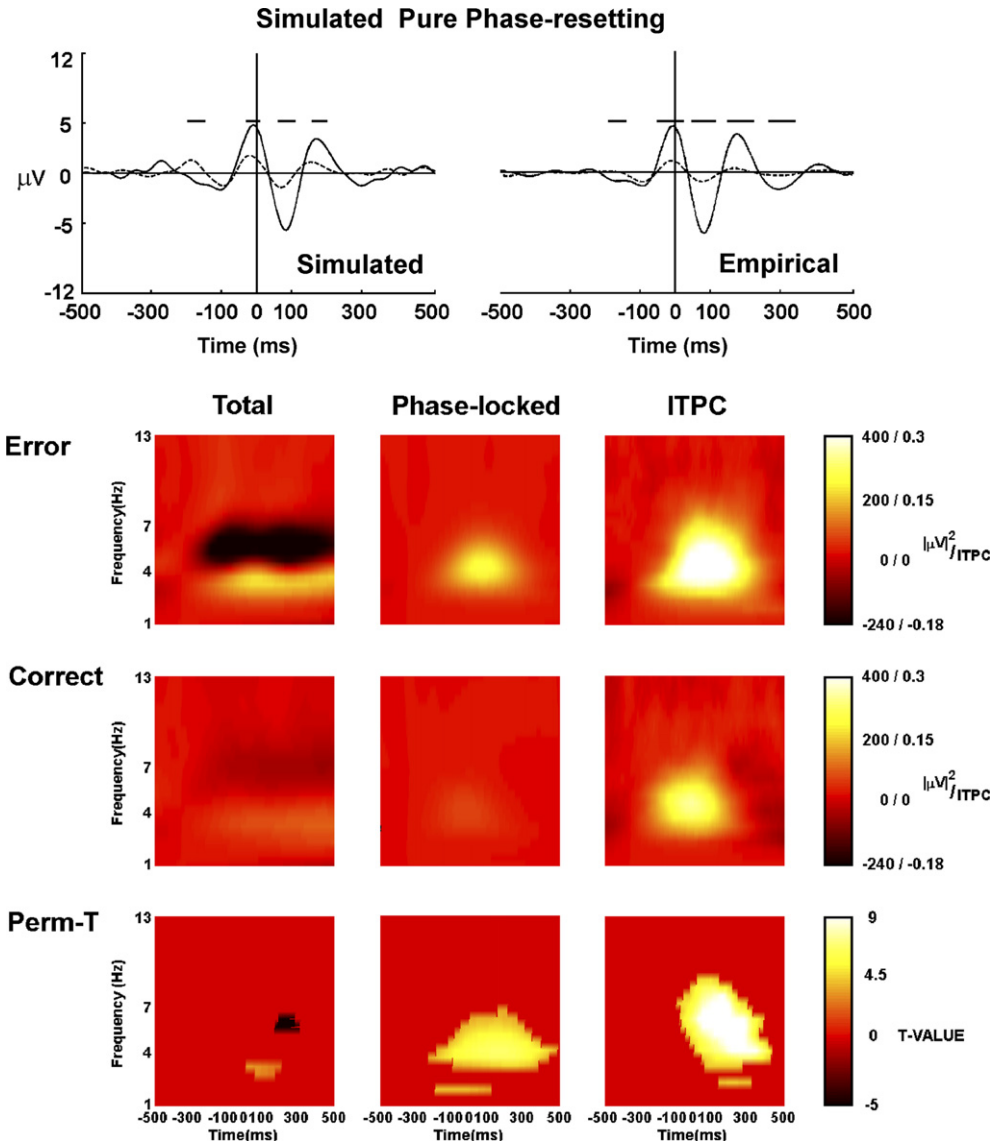

Fig. 6. Results of simulated pure phase-resetting hypothesis. Top panels: Grand-average narrow-band ERN waveforms for Error and Correct responses simulated according to the *pure phase-resetting hypothesis* (left). Grand-average narrow-band empirical ERN waveforms (right). Solid black line = Error responses, dashed black line = Correct responses, solid horizontal lines = time points containing statistically significant ($p < 0.05$, two-tailed) Error vs. Correct differences. Bottom panel: Baseline-corrected grand-average total power (left column), phase-locked power (center column) and ITPC (right column) responses for simulated Error (top row) and Correct data (middle row). Light colors indicate increases with respect to the pre-response baseline; dark colors indicate decreases. Bottom row: Error vs. Correct permutation *T*-test statistical comparisons for simulated data. Light colors indicate positive *T*-values; dark colors indicate negative *T*-values; intermediate colors indicate zero values. All non-zero *T*-values displayed in the figure are significant at the $p < 0.05$ (two-tailed) level.

phase-locked and ITPC differences were small and idiosyncratically located within the time–frequency plane.

3.6. Phase-resetting with enhancement simulations

Fig. 8 (top panels) shows narrow-band (3–15 Hz) filtered ERPs simulated according to the phase-resetting plus enhancement hypothesis (top left panel) and for the narrow-band empirical waveforms (top right panel). The morphology of the simulated waveforms is near identical to that of the empirical waveforms, both in terms of peak amplitudes and temporal spread. Significant Error vs. Correct amplitude differences occurred at the major waveform peaks for the simulated data (solid black lines, Fig. 8, top panel).

Fig. 8 (bottom panel) shows the time–frequency analyses of the simulated phase-resetting plus enhancement ERPs. Both Error (Fig. 8, bottom panel, top row) and Correct (Fig. 8, bottom panel, middle row) spectral responses have magnitudes and morphologies that are qualitatively similar to the spectral responses of the empirical waveforms. Total power (left column), phase-locked power (center column), and ITPC responses (right column) are substantially extended across time, and are distributed across the theta-band range (with some extension into the upper delta and lower alpha ranges) in a very similar

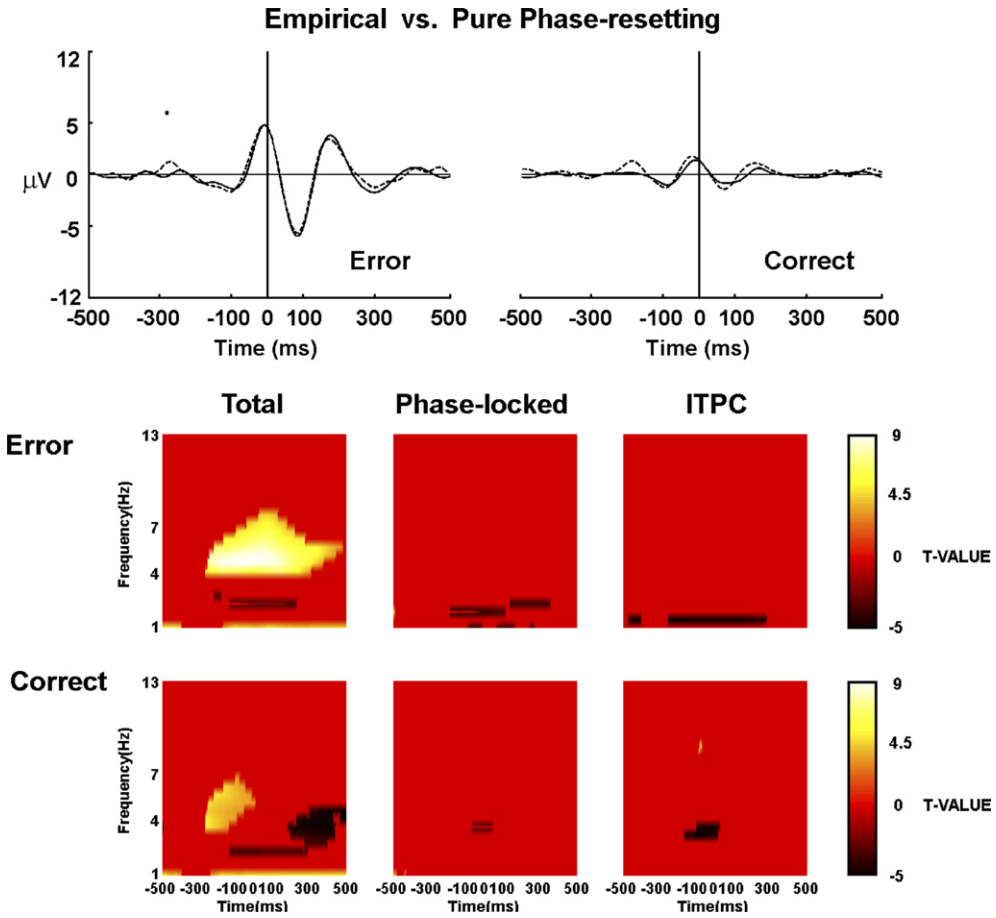

Fig. 7. Quantitative comparison of empirical data and simulated pure phase-resetting hypothesis. Top panel displays time–domain average waveforms: Solid black line = empirical data, dashed black line = simulated data, solid horizontal lines = time points containing statistically significant ($p < 0.05$, two-tailed) Empirical vs. Simulated differences. Lower panel displays permutation T-test statistical comparisons between empirical and pure *phase-resetting* time–frequency responses. Top row: Pure phase-resetting vs. empirical Error responses. Bottom row: Pure phase-resetting vs. empirical Correct responses. Light colors indicate positive T-values; dark colors indicate negative T-values; intermediate colors indicate zero values. All non-zero T-values displayed in the figure are significant at the $p < 0.05$ (two-tailed) level.

manner to the empirical responses. Furthermore, the spectral responses exhibit patterns of significant Error/Correct differences (Fig. 8, bottom panel, bottom row) comparable to the empirical differences shown in Fig. 3.

The qualitative similarities between the simulated phase-resetting plus enhancement ERN responses and the empirical responses were quantitatively confirmed by the permutation T-test comparisons (Fig. 9). Fig. 9 (top panels) compares the narrow-band filtered ERPs simulated according to the phase-resetting plus enhancement hypothesis to the narrow-band empirical waveforms for the Error (top left panel) and correct (top right panel) conditions. The two types of waveforms were not statistically different from each other at any time point. With respect to the time–frequency responses, the T-tests showed virtually no differences between phase-resetting plus enhancement and empirical Error/Correct responses (Fig. 9, bottom panel). The differences that did exist were limited to the total power comparisons over the upper delta and lower alpha frequency ranges, outside the range modeled by this simulation.

3.7. Non-phase-locked power

Fig. 10 (left column) shows the time–frequency representations of baseline-corrected Error trial non-phase-locked power for the empirical and three types of simulated data. The basic time–frequency pattern of the nonphase-locked power follows that of the corresponding total and phase-locked power for each data type. Empirical and phase-resetting with enhancement data all showed substantial increases in non-phase-locked activity; in contrast, pure phase-resetting data showed a decrease in non-phase-locked power. Classic data showed little-to-no increase in non-phase-locked activity, consistent with the high degree of phase-locking necessary for this simulation method to produce a reasonable ERN (see Section 3.7).

Statistical comparisons between non-baseline-corrected responses (not shown) revealed that non-phase-locked power was always significantly greater than phase-locked power ($p < 0.05$) for the empirical and all three types of simulated data. The large empirical difference between total and phase-locked power indicates that the bulk of the ERN

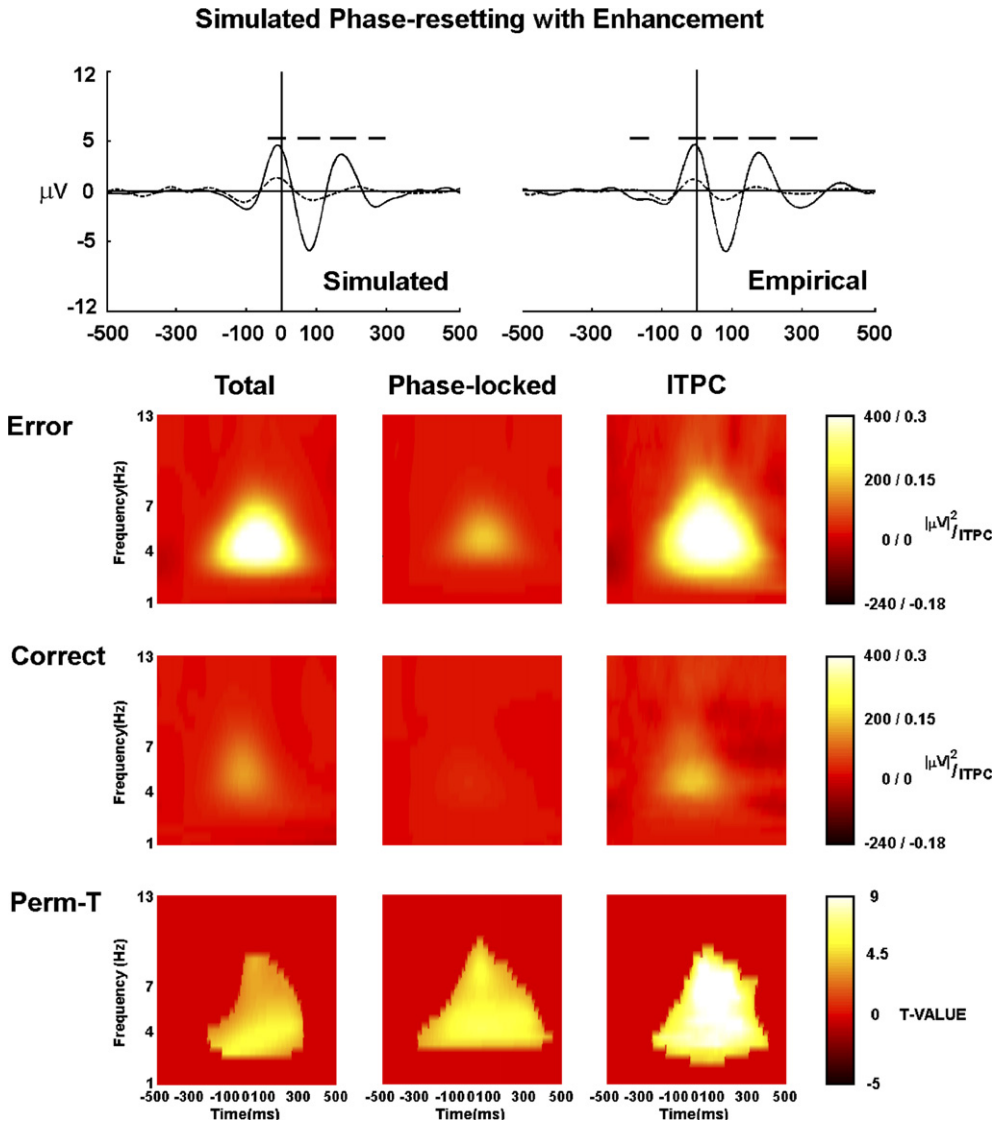

Fig. 8. Results of simulated phase-resetting with amplitude enhancement hypothesis. Top panels: Grand-average narrow-band ERN waveforms for Error and Correct responses simulated according to the *phase-resetting with enhancement hypothesis* (left). Grand-average narrow-band empirical ERN waveforms (right). Solid black line = Error responses, dashed black line = Correct responses, solid horizontal lines = time points containing statistically significant ($p < 0.05$, two-tailed) Error vs. Correct differences. Bottom panel: Baseline-corrected grand-average total power (left column), phase-locked power (center column) and ITPC (right column) responses for simulated Error (top row) and Correct data (middle row). Light colors indicate increases with respect to the pre-response baseline; dark colors indicate decreases. Bottom row: Error vs. Correct permutation *T*-test statistical comparisons for simulated data. Light colors indicate positive *T*-values; dark colors indicate negative *T*-values; intermediate colors indicate zero values. All non-zero *T*-values displayed in the figure are significant at the $p < 0.05$ (two-tailed) level.

total power spectrum is non-phase-locked with respect to the behavioral response (a button press), and does not survive the averaging process that creates the ERP. This large presence of non-phase-locked activity also explains the relatively low absolute (non-baseline-corrected) empirical ITPC magnitudes (< 0.4 units).

The comparison of baseline-corrected non-phase-locked vs. phase-locked power (Fig. 10, middle column), however, indicates that the changes in non-phase-locked and phase-locked power with respect to the baseline were not the same across empirical and simulated data. Empirical non-phase-locked power (Fig. 10, middle top panel) increased to a significantly greater degree than phase-locked power over the theta range during the majority of the ERN response (∼−350 to 150 ms).[5] In contrast, increases in classic non-phase-locked theta power (Fig. 10, middle column, second panel) were significantly less than classic phase-locked power increases. Pure phase-resetting non-phase-locked power (Fig. 10, middle column, third panel) actually decreased while phase-locked power increased in the theta range from ∼−300 to 500 ms. Only the phase-resetting

[5] It is not immediately clear why the comparison between empirical non-phase-locked and phase-locked power shows a rather abrupt change from significantly less to significantly greater power around -400 ms. This transition may simply reflect small, negligible fluctuations around baseline that are nonetheless highly reliable, and thus lead to significant *T*-values. Another possibility is that this transition reflects a small amount of stimulus-related phase-locked activity in the −500 to −400 ms interval.

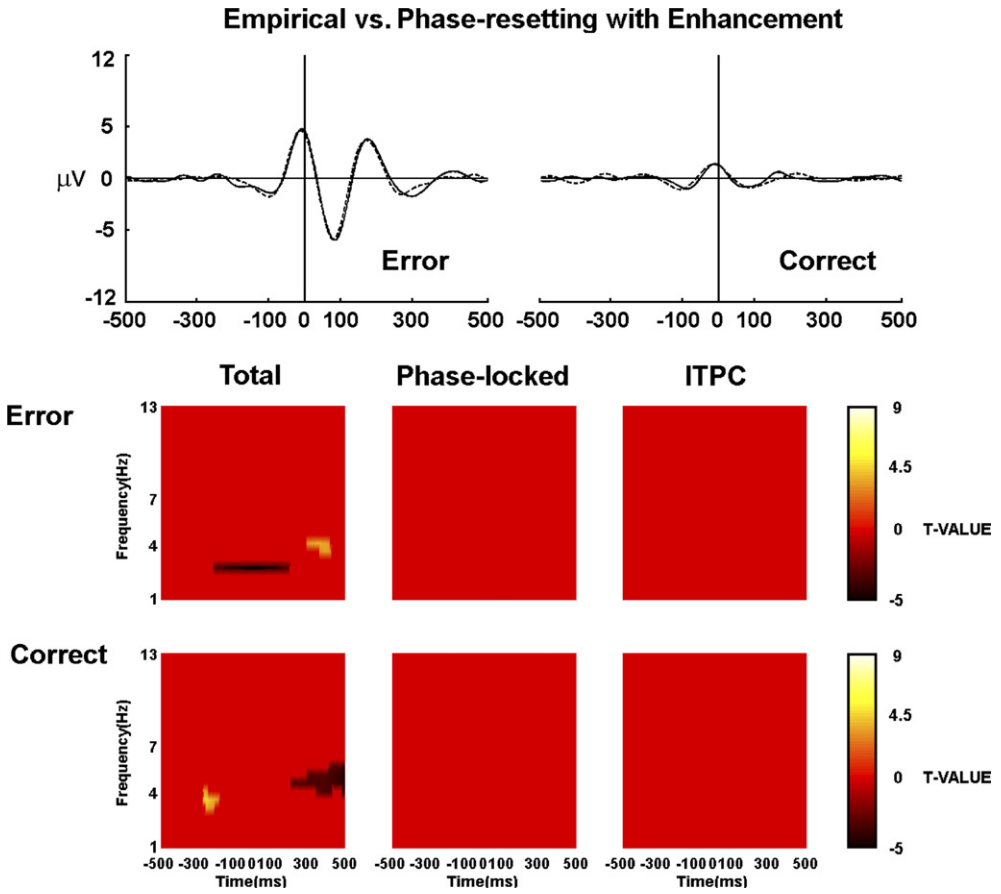

Fig. 9. Quantitative comparison of empirical data and simulated phase-resetting with enhancement hypothesis. Top panel displays time–domain average waveforms: Solid black line = empirical data, dashed black line = simulated data, solid horizontal lines = time points containing statistically significant ($p < 0.05$, two-tailed) Empirical vs. Simulated differences (note none were significant). Lower panel displays permutation T-test statistical comparisons between empirical and *phase-resetting with enhancement* time–frequency responses. Top row: Phase-resetting with enhancement vs. empirical Error responses. Bottom row: Phase-resetting with enhancement vs. empirical Correct responses. Light colors indicate positive T-values; dark colors indicate negative T-values; intermediate colors indicate zero values. All non-zero T-values displayed in the figure are significant at the $p < 0.05$ (two-tailed) level.

with enhancement simulation (Fig. 10, middle column, bottom panel) showed non-phase-locked versus phase-locked power increases, although these were restricted to the lower theta/upper delta range.

Fig. 10 (right column) displays time–frequency permutation-T maps comparing empirical vs. simulated baseline-corrected Error trial non-phase-locked power for all three ERN simulations. Empirical non-phase-locked power was significantly greater than classic and pure phase-resetting non-phase-locked power over the theta range. There were few differences between the empirical and phase-resetting with enhancement non-phase-locked power responses, further indicating the goodness of fit of this particular model to the empirical data.

4. Discussion

4.1. Evidence for the Phase-resetting with enhancement hypothesis of ERN generation

The empirical time–domain and time–frequency results (Sections 3.2, 3.3) support the hypothesis that the ERN emerges from the partial phase-locking of midfrontal theta-band EEG oscillatory activity. First, significant error-related post-response increases in spectral amplitude and ITPC were primarily restricted to the theta range for both Error and Correct trials. Second, a greater degree of activity was found for empirical Error versus Correct trials for the narrow-filtered ERP (Figs. 4–9) and all theta spectrum power and ITPC measures (Fig. 3). These Accuracy-related differences were located over midfrontocentral sites, with an onset of ≈150–200 ms prior to the button press that persisted up to 400 ms post-button press. Third, the empirical data were best modeled by data simulated according to the phase-resetting with enhancement model. Furthermore, this evidence was acquired through an analysis method that circumvents difficulties associated with the interpretation of time–frequency patterns (e.g., Yeung et al., 2004; see Sections 1.2, 1.3 and 1.4).

The simulation results presented in Section 3.4 appear to rule out the classic hypothesis. The classic simulations produced ERPs that fit the empirical narrow-band responses over the central peak of the ERN response, but could not fully account for the presence of neighboring oscillatory

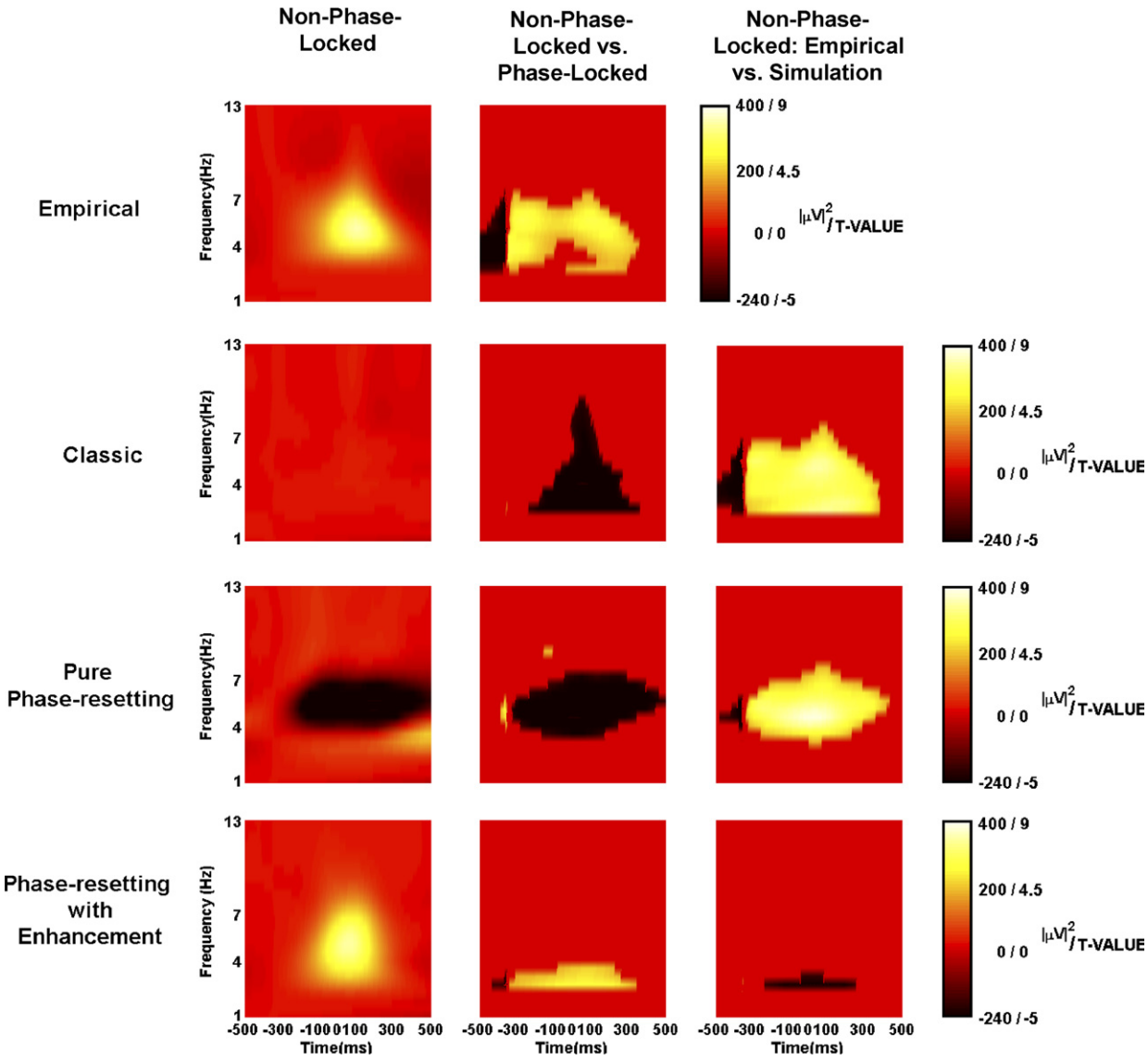

Fig. 10. Assessment of *Non-phase-locked power*. Left column: Baseline-corrected grand-average non-phase-locked power for Error trial empirical (top row), classic (second row), pure phase-resetting (third row), and phase-resetting plus enhancement (bottom row) data. Light colors indicate increases with respect to the pre-response baseline; dark colors indicate decreases. Middle column: Permutation *T*-test statistical comparisons between baseline-corrected Error trial non-phase-locked and phase-locked power for empirical (top row), classic (second row), pure phase-resetting (third row), and phase-resetting plus enhancement (bottom row) data. Right column: Permutation *T*-test statistical comparisons of Error trial non-phase-locked power between empirical and classic (second row), pure phase-resetting (third row), and phase-resetting plus enhancement (bottom row) data. Light colors indicate positive *T*-values; dark colors indicate negative *T*-values; intermediate colors indicate zero values. All non-zero *T*-values displayed in the figure are significant at the $p < 0.05$ (two-tailed) level. Significant differences within the −500 to −300 ms interval (which includes the baseline period) are likely due to low amplitude differences exhibiting exceedingly low variability and/or residual stimulus-related phase-locked activity.

peaks present in the empirical ERN waveform. This situation was not improved by increasing the phase-locking of the simulated classic signals, but instead indicates the limitations of the classic model. Time–frequency analyses reinforced the inadequacy of the classic model. Large theta-range differences in all three types of spectral power (total, phase-locked, non-phase-locked) were found between the empirical and classically simulated data. Such differences were present even though the empirical ERN values used to constrain the amplitudes of classical simulations were extracted from the data of individual subjects. Increasing the across-trial phase-locking, while increasing total power, phase-locked power, and ITPC, did not improve the overall fit of the classical model to the observed data. Interestingly, classic ITPC responses were rarely lower than empirical ITPC responses, and in some cases even exceeded the latter by a significant amount (Fig. 5). This supports Yeung et al.'s (2004) conclusion that a phasic response occurring with a relatively stable latency across trials can impose a dominant phase upon single-trial EEG signals.

The pure phase-resetting and phase-resetting plus enhancement simulations produced ERPs that were nearly

identical to the empirical narrow-band ERN, thus establishing the validity of these simulations. Pure phase-resetting also yielded phase-locked power and ITPC responses similar to their empirical counterparts. Pure phase-resetting, however, led to significant decreases in total and non-phase-locked power that were clearly not present in the empirical data (Figs. 1B, 6 and 7). By contrast, little-to-no power or ITPC differences were found between the empirical data and data simulated according to the phase-resetting with enhancement hypothesis (Fig. 9). The robustness of this fit with the empirical data strongly favors the phase-resetting with enhancement hypothesis over the classic and phase-resetting hypotheses of the ERN.

4.2. Evidence for a midfrontocentral theta source

The topography and time course of the spectral power and phase-locking observed in the present ERN data are consistent with those reported by Luu et al. (2004). The scalp topographies of total/phase-locked power and ITPC were highly similar, with a frontal-central midline maximum. This pattern is highly consistent with the hypothesis that the ERN arises from midfrontocentral EEG sources with respect to the motor response, and consistent with previous studies that have implicated the dorsal anterior cingulate cortex as the generator of the ERN (Dehaene et al., 1994; Luu and Tucker, 2001; Dikman and Allen, 2000). Moreover, the similarity of topography of total and phase-locked power makes less tenable the assumption that the phase-locked event-related activity is purely independent of and physiologically distinct from the background activity, and is consistent with findings that trial-to-trial variations in evoked activity can be accounted for by the dynamics of ongoing activity (e.g., Arieli et al., 1996).

4.3. Non-phase-locked theta activity

One notable feature of the present results is the large degree of non-phase-locked theta activity and activity increases present in the empirical data (see Section 3.7 and Fig. 10); the amount of non-phase-locked activity is much greater than the amount reported by Luu et al. (2004). This difference between the two studies may be due to the differences in task demands. In the present study, participants performed under reward and punishment feedback conditions that might recruit supplementary neural populations associated with the increased affective appreciation of error and correct responses. Participants also had motivation to self-correct their errors in order to avoid punishment or loss of reward. The motor implementation of this error correction may have contributed additional non-phase-locked activity to that observed here. These suggestions are supported by other findings that non-phase-locked oscillatory responses in different frequency ranges (alpha, beta, gamma) increase with cognitive task performance, motor activity, and affective evaluation (c.f. Pantev, 1995; Muller et al., 1999; Pfurtscheller, 1999; Rodriguez et al., 1999; Mima et al., 2001; Trujillo et al., 2005), but await further research.

4.4. Conclusion

The present results, along with those of Luu et al. (2004), suggest a mechanism of ERN generation that depends on the partial phase-resetting plus amplitude enhancement of ongoing theta activity in the anterior cingulate, which may be part of a broader limbic network generating theta activity relevant to learning and reward (Caplan et al., 2003). The present study extends the findings of Luu et al. (2004) by demonstrating theta-band error-correct differences using newer time–frequency methods. Use of the wavelet transform precludes the possibility that the present results arise out of artifacts (Yeung et al., 2004) associated with the band-pass filtering rectification method used by Luu et al. (2004). Problematic factors peculiar to wavelet transforms such as edge-effects were also carefully controlled for in the present analysis (Section 2.6).

The present study also extends the report of Yeung et al. (2004) by quantitatively comparing empirical data to data simulated according to the classic, pure phase-resetting, and phase-resetting with enhancement hypotheses, with spectral differences quantitatively assessed across time and frequency. This procedure provides a much stronger and unambiguous test between these hypotheses of ERN genesis. In addition, these findings were obtained even when matching error and correct EEG trials for confounding factors that can introduce differential variability into the EEG signals across Accuracy conditions (Section 2.4.1). Thus the present results suggest a veritable increase in theta activity surrounding the ERN, a portion of which is phase-reset during error processing.

On the other hand, the present results in no way suggest that all event-related activity need arise by such mechanisms, as activity in other cortical regions or evoked by different stimulus modalities may not necessarily show such phase-resetting (e.g., Mäkinen et al., 2005). Indeed, the methods and results reported in this paper are relevant not only to the ERN, but to all ERPs in general; they should be useful in resolving questions concerning the genesis of other ERP markers of cognition and behavior. Such future research should aim to uncover the neural conditions that lead to oscillatory versus phasic event-related EEG responses, as well as to further clarify the interaction of these mechanisms in the genesis of event-related EEG activity.

Acknowledgements

This research was supported in part by a US Department of Education Jacob K. Javits Fellowship, a

University of Arizona Institute for Collaborative Bioresearch (BIO5) Graduate Research Award, and an American Psychological Association Dissertation Research Award to L.T.T.; and a grant from the McDonnell-Pew Program in Cognitive Neuroscience to J.J.B.A. The authors are grateful to Ziya V. Dikman for assistance with data collection, data analysis, and helpful comments on drafts of this manuscript. The authors also wish to thank two anonymous reviewers for their helpful critiques on an earlier draft of this paper. Address correspondence to Logan Trujillo or John JB Allen, Department of Psychology, P.O. Box 210068, Tucson, AZ 85721-0068. Email: logant@u.arizona.edu or jallen@u.arizona.edu.

References

Addison, PS. The illustrated wavelet transform handbook: Introductory theory and applications in science, engineering, medicine, and finance. Bristol, UK: IOP Publishing Ltd.

Arieli A, Sterkin A, Grinvald A, Aertsen A. Dynamics of ongoing activity: explanation of the large variability in evoked cortical responses. Science 1996;273:1868–71.

Badgaiyan RD, Posner MI. Mapping the cingulate cortex in response selection and monitoring. Neuroimage 1998;7:255–60.

Basar E. Brain function and oscillations. Berlin: Springer; 1991.

Basar-Eroglu C, Basar E, Demiralp T, Schurman M. P300-response: possible psychophysiological correlations in delta and theta frequency channels. A review. Int J Psychophysiol 1992;13:161–79.

Burgess AP, Gruzelier JH. Methodological advances in the analysis of event-related desynchronization data: reliability and robust analysis. In: Pfurscheller G, Lopes da Silva FH, editors. Hand book of electroencephalography and clinical neurophsyiology, revised series, Vol. 6. New York: Elsevier Science; 1999. p. 139–58.

Buzsáki G, Leung L-WS, Vanderwolf CH. Cellular bases of hippocampal EEG in the behaving rat. Brain Res Rev 1983;6:139–71.

Caplan JB, Madsen JR, Schulze-Bonhage A, Aschenbrenner-Scheibe R, Newman EL, Kahana MJ. Human theta oscillations related to sensorimotor integration and spatial learning. J Neurosci 2003;23:4726–36.

Carter CS, Braver TS, Barch DM, Botvinick MM, Noll D, Cohen JD. Anterior cingulate cortex, error detection, and the online monitoring of performance. Science 1998;280:747–9.

Dikman ZV, Allen JJB. Error monitoring during reward and avoidance learning in high- and low-socialized individuals. Psychophysiology 2000;37:43–54.

Dehaene S, Posner MI, Tucker DM. Localization of a neural system for error detection and compensation. Psychol Sci 1994;5:303–5.

Delorme A, Makeig S. EEGLAB: an open source toolbox for analysis of single-trial EEG dynamics including independent components analysis. J Neurosci Methods 2004;134:9–21.

Falkenstein M, Hohnsbein J, Hoorman J, Blanke L. Effects of crossmodal divided attention on late ERP components. II. Error processing in choice reaction time tasks. Electroencephalogr Clin Neurophysiol 1991;78:447–55.

Falkenstein M, Hoorman J, Hohnsbein J. ERP components in Go/Nogo tasks and their relation to inhibition. Acta Psychologica 1999;101(2–3): 267–91.

Falkenstein M, Hoorman J, Christ S, Hohnsbein J. ERP components on reaction errors and their functional significance: a tutorial. Biol Psychol 2000;51:87–107.

Freund TF, Buzaki G. Interneurons of the hippocampus. Hippocampus 1996;6:347–470.

Gehring WJ, Gratton G, Coles MGH, Meyer DE, Donchin E. Probability effects on stimulus evaluation and reponse processes. J Exp Psychol Hum Percept Perform 1992;18(1):198–216.

Gehring WJ, Goss B, Coles MGH, Meyer DE, Donchin E. A neural system for error detection and compensation. Psychol Sci 1993;4:385–90.

Gehring WJ, Himle J, Nisenson LG. Action monitoring dysfunction in obsessive-compulsive disorder. Psychol Sci 2000;11:1–6.

Gehring WJ, Willoughby AR. The medial frontal cortex and the rapid processing of monetary gains and losses. Science 2002;295: 2279–82.

Gehring WJ, Willoughby AR. Are all medial frontal negativities created equal? Toward a richer empirical basis for theories of action monitoring. In: Ullsperger M, Falkenstein M, editors. Errors, conflict, and the brain. Current opinions on performance monitoring. Leipzig: MPI of Cognitive Neuroscience; 2004. p. 14–20.

Leigh RJ, Zee DS. The neurology of eye movements. 2nd ed. Philadelphia: F.A. Davis; 1991.

Luu P, Tucker DM. Regulating action: alternating activation of human prefrontal and motor cortical networks. Clin Neurophysiol 2001;112:1295–306.

Luu P, Tucker DM, Derryberry D, Reed M, Poulsen C. Activity in human medial frontal cortex in emotional evaluation and error monitoring. Psychol Sci 2003;14:47–53.

Luu P, Tucker DM, Makeig S. Frontal midline theta and the error-related negativity; neurophysiological mechanisms of action regulation. Clin Neurophysiol 2004;115:1821–35.

Klimesch W, Schack B, Schabus M, Doppelmayr M, Gruber W, Sauseng P. Phase-locked alpha and theta oscillations generate the P1–N1 complex and are related to memory performance. Cogn Brain Res 2004;19:302–16.

Makeig S, Westerfield M, Jung T-P, Enghoff S, Townsend J, Courschene E, et al. Dynamic brain sources of visual evoked responses. Science 2002;295:609–94.

Mäkinen V, Tiitinen H, May P. Auditory event-related responses are generated independently of ongoing brain activity. Neuroimage 2005;24:961–8.

Mallat S. A wavelet tour of signal processing. London: Academic Press; 1999.

Miltner WHR, Braun CH, Coles MGH. Event-related brain potentials following incorrect feedback in a time-estimation task: evidence for a ''generic'' neural system for error detection. J Cogn Neurosci 1997;9:787–97.

Mima T, Oluwatimilehin T, Hiraoka T, Hallet M. Transient interhemispheric neuronal synchrony correlates with object recognition. J Neurosci 2001;21:3942–8.

Muller MM, Keil A, Gruber T, Elbert T. Processing of affective pictures modulates right-hemispheric gamma band activity. Clin Neurophysiol 1999;110:1913–20.

Nichols TE, Holmes AP. Nonparametric permutation tests for functional neuroimaging: a primer with examples. Human Brain Mapping 2001;15:1–25.

Pantev C. Evoked and induced gamma-band activity of the human cortex. Brain Topogr 1995;7:321–30.

Pfurtscheller G. EEG event-related desynchonization (ERD) and event-related synchronization (ERS). In: Niedermayer E, Lopes Da Silva F, editors. Electroencephalography: basic principles, clinical applications, and related fields. 4th ed. Baltimore: Williams and Wilkins; 1999. p. 958–67.

Rodriguez E, George N, Lachaux J-P, Martinerie J, Renault B, Varela FJ. Perception's shadow: long-distance synchronization of human brain activity. Nature 1999;397:430–3.

Ruschow M, Grothe J, Spitzer M, Keifer M. Human anterior cingulate cortex is activated by negative feedback: evidence from event-related potentials in a guessing task. Neurosci Lett 2002;325:203–6.

Semlitsch HV, Anderer P, Schuster P. A solution for reliable and valid reduction of ocular artifacts, applied to the P300 ERP. Psychophysiology 1986;23:695–703.

Tallon-Baudry C, Bertrand O, Delpuech C, Pernier J. Oscillatory gamma band (30–70 Hz) activity induced by visual search task in human. J Neurosci 1997;17:722–34.

Trujillo LT, Peterson MA, Kasniak AW, Allen JJB. EEG phase synchrony differences across visual perception conditions may depend on recording and analysis methods. Clin Neurophysiol 2005;116:172–89.

Wang C, Ulbert I, Schomer DL, Marinkovic K, Halgren E. Responses of human anterior cingulate cortex microdomains to error detection, conflict monitoring, stimulus-response mapping, familiarity, and orienting. J Neurosci 2005;25:604–13.

Yeung N, Bogacz R, Holroyd CB, Cohen JD. Detection of synchronized oscillations in the electroencephalogram: an evaluation of methods. Psychophysics 2004;41:822–32.